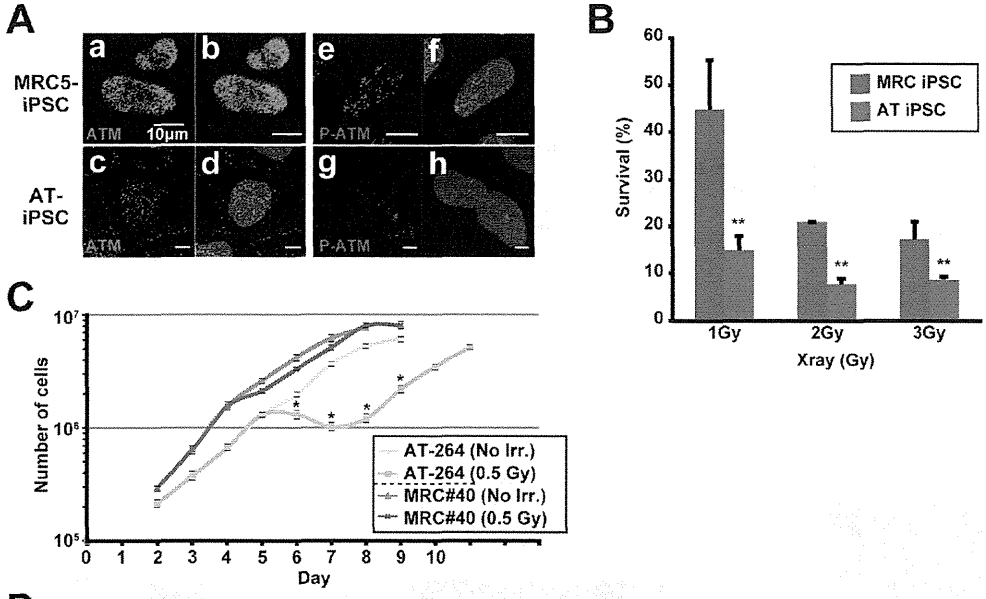

D

Cell	Passage	Irradiation (Gy)	Mode	Karyotype
MRCiPS#16	P59	0	46(50)	46,XY[20]
		0.5	46(48),47(2)	46,XY[19] 46,XY,chtb(14)(q24)[1]
		1.0	45(1),46(49)	46,XY[19] 45,XY,dic(2;2)(p23;P25)[1]
MRCiPS#25	P43	0	46(50)	46,XY[20]
		0.5	46(50)	46,XY[20]
		1.0	46(50)	46,XY[20]
MRCiPS#40	P62	0	46(50)	46,XY[20]
		0.5	46(50)	46,XY[20]
		1.0	46(50)	46,XY[20]
ATiPS-262	P76	0	46(50)	46,XY[20]
		0.5	46(50)	46,XY[20]
		1.0	46(50)	46,XY[20]
ATiPS-263	P84	0	46(50)	46,XY[20]
		0.5	46(50)	46,XY[20]
		1.0	46(50)	46,XY[20]
ATiPS-264	P81	0	46(50)	46,XY[20]
		0.5	46(50)	46,XY[20]
		1.0	44(1),46(48),49(1)	46,XY[17] 46,XY,t(18;19)(q12.2;p13.3)[1] 44,XY,qr(1;3)(p22;p21),-5,-9,chtb(9)(p22),chtb(16)(q11.1),-22,+2mar[1] 49,X,-Y,add(1)(q42),add(4)(q?25),chtb(8)(p21),-14,chtb(17)(p11.2),+5mar[1]
ATiPS-024	P85	0	46(50)	46,XY[20]
		0.5	46(50)	46,XY[18] 46,XY,chtb(17)(q?23) x 2[1] 46,XY,dic(1;2)(q44;p25),mar[1]
		1.0	46(50)	46,XY[20]

Figure 5 | Effect of X-ray irradiation on AT-iPS cells. (A). Immunocytochemistry of ATM (a and c: green) and phosphorylated ATM (e and g: red, labeled as P-ATM). AT-iPS (ATiPS-262) and MRC5-iPS (MRCiPS#16) cells were analyzed at 5 min after 0.5-Gy irradiation. (a), (b), (e) and (f): MRC5-iPS cells; (c), (d), (g) and (h): AT-iPS cells (ATiPS-262). (b) and (d): Merge of ATM and DAPI stain; (f) and (h): Merge of phosphorylated ATM and DAPI stain. (B). Dose effect of irradiation on AT-iPS cells (ATiPS-262, -263, -264, -024) and MRC5-iPS cells (MRCiPS#16, #25, #40). Frequencies of viable cells were calculated from the cell number on 2 days after irradiation at the indicated doses to estimate growth retardation and cell survival. Data for AT-iPS and MRC5-iPS cells were obtained from the quadruplicate and triplicate independent experiments, respectively. Nonirradiated cells were regarded as equal to 100%. Asterisks (**) denote statistically significant with $p < 0.01$ by student's t-test (1 Gy, $p = 1.2 \times 10^{-3}$; 2 Gy, $p = 5.1 \times 10^{-6}$; 3 Gy, $p = 2.8 \times 10^{-3}$). (C). Effect of irradiation on growth of AT-iPS and MRC5-iPS cells. iPS cells were irradiated at 0.5 Gy on Day 4. Cell number was calculated at the indicated days after cells (10^5) were seeded on Day 0. Non-irradiated (No Irr.) iPS cells were also shown for control. Asterisks (*) denote statistically significant between irradiated and nonirradiated cells with $p < 0.01$ by student's t-test (Day 6, $p = 3.2 \times 10^{-4}$; Day 7, $p = 6.1 \times 10^{-6}$; Day 8, $p = 3.8 \times 10^{-6}$; Day 9, $p = 9.9 \times 10^{-7}$). (D). Irradiation effect on karyotypes of AT-iPS cells. Mode: 50 cells were analyzed for chromosomal aneuploidy. Number of cells with each chromosomal number is shown in Parentheses. Karyotype: For karyotypic analysis, 20 cells were analyzed and the number of karyotype was shown in brackets.

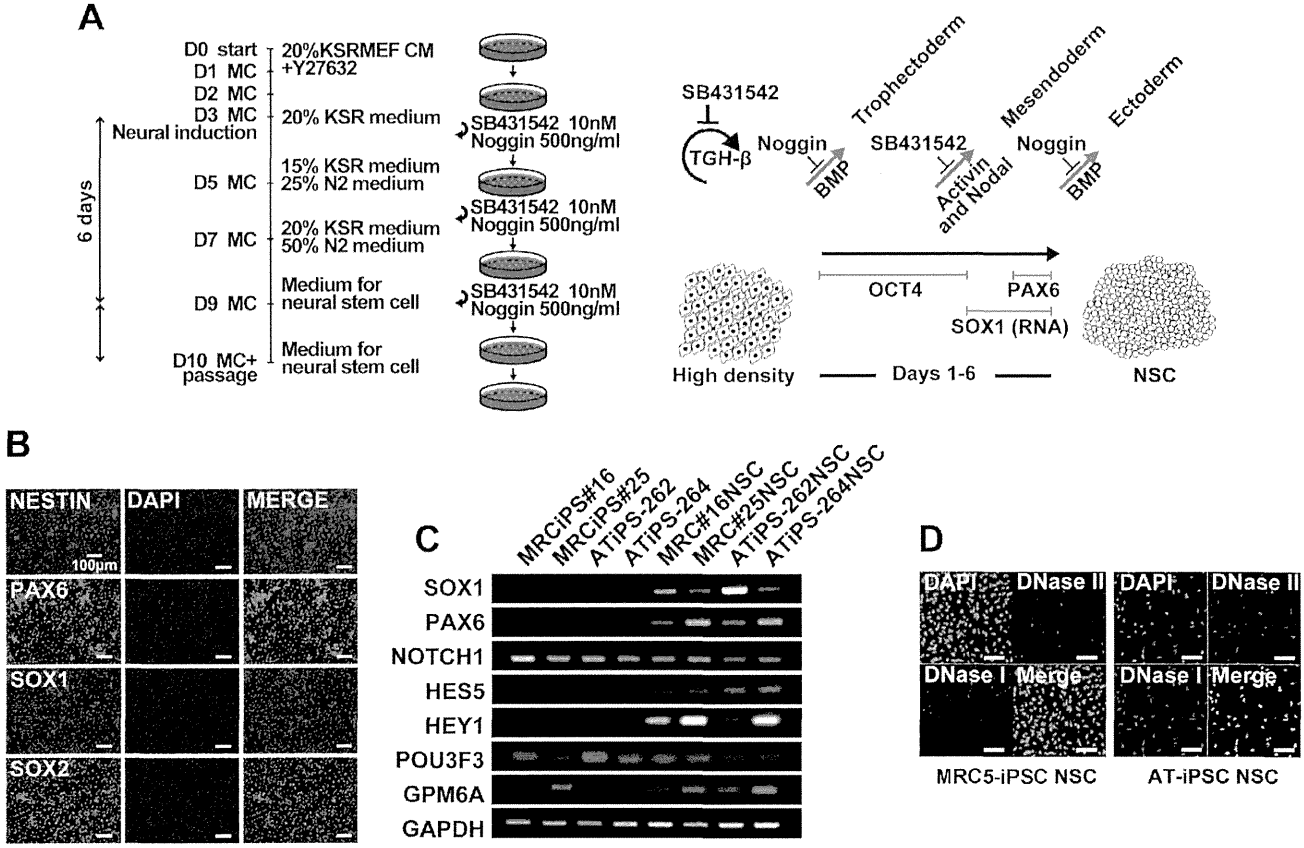

Figure 6 | Neural differentiation of AT-iPS cells. (A).Protocol for neural differentiation of AT-iPS cells. Neural differentiation of iPS cells was performed according to the standard protocol[37]. MC: Medium change. (B). Immunocytochemistry of AT-iPS cells (ATiPS-262). (C). RT-PCR analysis on AT-iPS cells (ATiPS-262, ATiPS-264) and MRC5-iPS cells (MRCiPS#16, MRCiPS#25) after neural differentiation. Primers are listed in Supplemental Table S1. (D). Apoptosis of AT-iPS cells after neural differentiation. Apoptosis was detected by the ApopTag ISOL Dual Fluorescence Apoptosis Detection Kit (DNase Types I & II) APT1000 (Millipore). Left panels: neural differentiation of MRC5-iPS cells (MRCiPS#25), right panels: neural differentiation of AT-iPS cells (ATiPS-262).

(Supplemental Figure S7B, C). These results indicate that AT-iPS cells have higher radiation sensitivity than the intact iPS cells when growth characteristics are considered.

Karyotypic analyses of AT-iPS cells and MRC5-iPS cells were performed after X-ray irradiation, and did not reveal any significant difference in the radiation sensitivity. Most cells analyzed showed an intact chromosomal pattern even after longer cultivation (ATiPS-264: Passage 81 and 20 months, ATiPS-024: Passage 86 and 22 months). Only low frequencies of chromosomal abnormalities such as chromosomal loss and amplification, deletion, and translocation were detected in AT-iPS cells; MRC5-iPS cells showed similar results (Figure 5D).

Neural differentiation of iPS cells. Since one of the most common symptoms in patients with ataxia telangiectasia is neural impairment, we investigated neural differentiation of AT-iPS cells (ATiPS-262 and -264) and MRC5-iPS cells (MRCiPS#16 and #25) (Figure 6A). AT-iPS cells exhibited neural phenotypes by morphological analysis, immunocytochemistry (Figure 6B), and RT-PCR analysis (Figure 6C, Supplemental Figure S8), and no significant difference between AT-iPS cells and MRC5-iPS cells were detected. However, apoptosis significantly increased after neural differentiation of AT-iPS cells, compared with MRC5-iPS cells (Figure 6D). We obtained consistent results from all iPS cells examined.

Discussion

Human pluripotent stem cells deficient for the ATM gene have successfully been generated in two ways: Disruption of the ATM gene in human ES cells by genetic manipulation with bacterial artificial chromosome and derivation of disease-specific iPS cells from patients with ataxia telangiectasia[11–13]. The ATM-deficient pluripotent stem cells serve as disease model cells for clarification of pathogenic mechanisms and for screening novel compounds to treat the disease. In this study, we generated iPS cells from fibroblasts (AT1OS) of a human AT patient, and compared them with those from a healthy donor. The AT-iPS cells exhibited the same proliferation activity as wild type-iPS cells (WT-iPS cells), a gene expression profile characteristic of pluripotent stem cells such as ES cells and WT-iPS cells, the capability to differentiate into all three germ layers, and hypersensitivity in growth characteristics to X-ray irradiation. Apoptosis could be induced upon neural differentiation of AT-iPS cells. These results indicate that the established cells kept both characteristics of pluripotent stem cells and *ATM*-deficient cells.

Though normal ATM function was not a prerequisite for the establishment and maintenance of iPS cells, the reprogramming efficiency of the fibroblasts derived from an AT patient was extremely low, suggesting indirect roles of ATM in the somatic reprogramming process. One of the major targets of ATM is p53[14], and ATM-dependent phosphorylation is directly responsible for p53 activation. ATM and p53 are two proteins that are believed to play a major role in maintaining the integrity of the genome. In spite of having the related function of maintaining the integrity of the genome, p53 is known to serve as a barrier in iPS cell generation. Genetic ablation or decreased amounts of p53 remarkably increases reprogramming efficiency in mouse and human somatic cells[15–19]. Thus, ATM and p53

appear to have opposite roles on the reprogramming of differentiated cells to pluripotent cells. ATM kinase phosphorylates a broad range of substrates, and is involved in a wider range of safeguard systems than p53, such as DNA repair, apoptosis, G1/S, intra-S checkpoint and G2/M checkpoints. Thus, p53-independent reprogramming processes may have a crucial need for some ATM functions, and other phosphatidyl-inositol 3-kinase like enzymes, such as ATR, may partially compensate the ATM-deficiency.

Alternatively, telomere damage may explain the low reprogramming efficiency found in AT-derived fibroblasts. Telomeres found at the ends of eukaryotic chromosomes prevent their erosion, facilitate the recruitment of telomere-binding factors and stop the activation of the DNA damage response pathways. In humans, *ATM* deficiency results in accelerated telomere loss, and T lymphocytes derived from AT-patients exhibit frequent telomeric fusions[20]. Mouse cells with short telomeres cannot be reprogrammed to iPS cells despite their normal proliferation rates, probably reflecting the existence of 'reprogramming barriers' that abort the reprogramming of cells with uncapped telomeres[21,22].

Unexpectedly, we found that AT-iPS cells did not show any chromosomal instability *in vitro*, i.e., maintenance of intact chromosomes was observed after 80 passages (560 days). Even after X-ray irradiation at low dose, the most of AT-iPS cells still maintained an intact karyotype. In contrast, the parental fibroblastic cell line, AT1OS, showed frequent chromosomal abnormalities, such as deletion, addition and translocation. However, the AT-iPS cells still exhibited hypersensitivity to X-ray irradiation in the growth profile, which are major characteristics of ATM-deficient cells. These results indicate that AT-iPS cells maintain the defective response to ionizing irradiation, but that the defects do not affect maintenance of intact chromosomes.

What are the causes of the differences in the chromosomal stability between AT-iPS cells and AT1OS cells, the source of AT-iPS cells? The major difference between iPS cells and somatic cells may be the ability to undergo unlimited self-renewal. Somatic cells usually have limited growth potential, gradually decline with advancing age, and finally fall into senescence. In contrast, pluripotent stem cells are characterized by unlimited self-renewal and the ability to generate differentiated functional cell types. One of the causes of immortality is the presence of a terminal DNA polymerase capable of synthesizing telomeres, and somatic cell mortality is the result of a progressive loss of the telomeric DNA because of the absence of the immortalizing polymerase. The function of telomerase in terminal DNA elongation is necessary in order to overcome the "end-replication problem" whereby conventional DNA polymerases cannot fully replicate linear DNAs[23]. Telomere erosion (by 50–100 bp per cellular division) limits the replicative capacity of the majority of somatic cells, which do not express active telomerase[24]. In humans, *ATM* deficiency results in accelerated telomere loss in somatic cells, and T lymphocytes derived from AT patients exhibit frequent chromosomal instability[20].

Response to oxidative stress may be one of the causes of the accelerated telomere loss. It has been suggested that somatic cells, such as fibroblasts and neuronal cells from AT patients are in a chronic state of oxidative stress, which could contribute to their enhanced telomere shortening[25]. ATM protein is suggested to have a role in the prevention or repair of oxidative damage to telomeric DNA, and enhanced sensitivity of telomeric DNA to oxidative damage in AT cells results in accelerated telomere shortening and chromosomal instability. Further study using telomerase inhibitors and anti-oxidants using the human AT-iPS cells may clarify the cause of the difference between somatic cells and iPS cells derived from AT patients.

The number of single-nucleotide mutations per cell genome was estimated from 22 human iPS cells by extensive exome analysis on protein-coding sequences[26]. The exome analysis on the AT-iPS cell lines from 17 to 27 passages after the establishment in this study included not only coding but also untranslated, non-coding RNA, and their adjacent regions, covering up to 93.9 Mb. The number of observed coding mutations during reprogramming was comparable or smaller in all the three lines than those reported by the preceding study[26], supporting a genetic stability of the AT-iPS cells.

AT is characterized by early onset progressive cerebellar ataxia, oculocutaneous telangiectasia, susceptibility to bronchopulmonary disease, and lymphoid tumors. The pathologic tissues are generally not easily accessible, resulting in a substantial disadvantage for medical and biological studies of the pathogenesis of the disease and for development of novel therapeutic interventions. Generation of *Atm*-deficient mice partially overcomes such difficulties. However, oculocutaneous telangiectasias and histological evidence of neuronal degeneration, which are characteristics of human AT patients, have not seen in these mice, suggesting that the mouse model for AT is limited. Thus, the established human AT-iPS cells described in this study show promise as a tool for clarifying the pathogenesis of AT, and may facilitate development of drugs that inhibit ataxia and hypersensitivity to ionizing radiation.

Methods

Ethical statement. Human cells in this study were performed in full compliance with the Ethical Guidelines for Clinical Studies (2008 Notification number 415 of the Ministry of Health, Labor, and Welfare). The cells were banked after approval of the Institutional Review Board at the National Institute of Biomedical Innovation (May 9, 2006).

Human cells. AT1OS cells were obtained from a ten-year-old Japanese boy (JCRB Cell Bank, Osaka, Japan). The patient history is contained in the original report[27]. The patient was referred to the hospital because of progressive cerebellar ataxia and repeated upper respiratory infection. He raised his head well at 5 months and walked alone at 14 months of age. At the age of 2 years, his parents first noticed his tottering gait. He suffered from severe suppurative tympanitis at 4 years of age, since then he was recurrently afflicted with upper respiratory infections. Before school age, he had already developed a progressive ataxic gait. At the age of 10 years, he could walk alone only a short distance. The neurological examination revealed hyporeflexia, choreoathetosis, oculomotor apraxia and cerebellar dysarthria. Telangiectasia was seen in his bulbar conjunctivae. He showed mild mental retardation (IQ, 72). X-ray computed tomography revealed the fourth ventricular enlargement, suggesting mild cerebellar atrophy. Laboratory tests disclosed a decreased serum level of IgA (17 mg/dl) and a markedly elevated level of α-fetoprotein (560 ng/ml). Serum IgE and IgM were within normal levels. His parents are first cousins.

AT1OS cells were cultured in culture dishes (100 mm, Becton Dickinson). All cultures were maintained at 37°C in a humidified atmosphere containing 95% air and 5% CO_2. When the cultures reached subconfluence, the cells were harvested with a Trypsin-EDTA solution (cat# 23315, IBL CO., Ltd, Gunma, Japan), and re-plated at a density of 5×10^5 cells in a 100-mm dish. Medium changes were carried out twice a week thereafter. MRC5-iPS cells were maintained on irradiated MEFs as previously described[28,29]. MRC5iPS#16 (Fetch), MRC5iPS#25 (Tic), and MRC5iPS#40 (Skipper) were used as controls for AT-iPS cells. MRC5 (ATCC, CCL-171), a parental cell of MRC5-iPS cells, is from lung fibroblasts of 14-week fetus (Caucasian male).

Generation of iPS cells. AT-iPS cells were generated according to the method as previously described[28]. Briefly, to produce VSV-G (vesicular stomatitis virus G glycoprotein) retroviruses, 293FT cells (Invitrogen) were plated at 2×10^6 cells per 10-cm culture dish with DMEM supplemented with 10% FBS, and incubated overnight. On the next day, the cells were co-transfected with pMXs-OCT4, SOX2, KLF4 or c-MYC, pCL-GagPol, and pHCMV-VSV-G vectors using the TransIT-293 reagent (Mirus Bio LLC, Madison WI). The virus-containing supernatants were collected 48 h after incubation. The supernatants were filtered through a 0.45 μm pore-size filter, centrifuged, and then resuspended in DMEM supplemented with 4 μg/ml polybrene (Nacalai Tesque, Kyoto, Japan). Human AT1OS cells were seeded at 1.0×10^5 cells per well of 6-well plate 24 h before infection. A 1 : 1 : 1 : 1 mixture of OCT3/4, SOX2, KLF4, and c-MYC viruses was added to AT1OS cells[28–31]. The retrovirus carrying the EGFP gene was infected to estimate infection efficiency in a separate experiment. One-half of the medium was changed every day and colonies were picked up at around day 28.

RT-PCR. Total RNA was isolated from cells using the TRIzol (Invitrogen) or the RNeasy Plus Mini Kit (Qiagen). cDNA was synthesized from 1 μg of total RNA using Superscript III reverse transcriptase (Invitrogen) with random hexamers according to the manufacturer's instructions. Template cDNA was PCR-amplified with gene-specific primer sets (Supplemental Table S1).

Quantitative RT-PCR. RNA was extracted from cells using the RNeasy Plus Mini kit (Qiagen). An aliquot of total RNA was reverse transcribed using an oligo (dT) primer. For the thermal cycle reactions, the cDNA template was amplified (ABI PRISM

7900HT Sequence Detection System) with gene-specific primer sets using the Platinum Quantitative PCR SuperMix-UDG with ROX (11743-100, Invitrogen) under the following reaction conditions: 40 cycles of PCR (95°C for 15 s and 60°C for 1 min) after an initial denaturation (95°C for 2 min). Fluorescence was monitored during every PCR cycle at the annealing step. The authenticity and size of the PCR products were confirmed using a melting curve analysis (using software provided by Applied Biosystems) and a gel analysis. mRNA levels were normalized using GAPDH as a housekeeping gene.

Western blot analysis. Western blot analysis of total cell lysate for p53 and phospho-p53(Ser15) and of nuclear fractions for ATM was performed as described[32]. The membrane filter was probed with the antibodies to p53 (Enzo Life Sci., BML-SA293), phosphor-p53 (S15) (Cell signaling, #9284), and ATM (MBL, PM026), and then incubated with HRP-conjugated antibody to rabbit IgG. The protein signals were detected by ECL detection (Amersham).

Immunocytochemical analysis. Cells were fixed with 4% paraformaldehyde in PBS for 10 min at 4°C. After washing with PBS and treatment with 0.2% trypsin in PBS (PBST) for 10 min at 4°C, cells were pre-incubated with blocking buffer (10% goat serum in PBS) for 30 min at room temperature, and then reacted with primary antibodies in blocking buffer for 12 h at 4°C. Followed by washing with 0.2% PBST, cells were incubated with secondary antibodies; anti-rabbit or anti-mouse IgG conjugated with Alexa 488 or 546 (1 : 300) (Invitrogen) in blocking buffer for 1 h at room temperature. Then, the cells were counterstained with DAPI and mounted.

Karyotypic analysis. Karyotypic analysis was contracted out at Nihon Gene Reserch Laboratories Inc. (Sendai, Japan). Metaphase spreads were prepared from cells treated with 100 ng/mL of Colcemid (Karyo Max, Gibco Co. BRL) for 6 h. The cells were fixed with methanol : glacial acetic acid (2 : 5) three times, and dropped onto glass slides (Nihon Gene Reserch Laboratories Inc.). Chromosome spreads were Giemsa banded and photographed. A minimum of 10 metaphase spreads were analyzed for each sample, and karyotyped using a chromosome imaging analyzer system (Applied Spectral Imaging, Carlsbad, CA).

Quantitative fluorescence in situ hybridization (Q-FISH). We measured telomere length by Q-FISH analysis as previously described[33–35]. The parental cells and iPS cells were subjected to telomere measurements by the telomere fluorescent intensities of the p- and q-arms of all the chromosomes in the metaphase spread individually. The telomere lengths were determined by the median telomere fluorescent unit values.

Exome sequencing. Approximately 2.0 μg of genomic DNA from each cell sample was sonicated to give a fragment size of 200 bp on a Covaris S220 instrument. After 5–6 cycles of PCR amplification, capture and library preparation were performed with Agilent SureSelect Human All Exon V4 + UTRs + lincRNA (80 Mb), followed by washing, elution, and additional 10-cycle PCR. Enriched libraries were sequenced on an Illumina HiSeq 1000 operated in 101-bp paired-end mode. Image analyses and base calling on all lanes of data were performed using CASAVA 1.8.2 with default parameters.

Read mapping and variant analysis. Reads from each sample were first trimmed by removing adapters and low quality bases at ends using Trimmomatic 0.22 and then aligned to the hs37d5 sequence (hg19 and decoy sequences) using the Burrows-Wheeler Aligner 0.6.2. Uniquely mapped reads were selected by a custom script, converted from sam to bam using SAMtools 0.1.18, and processed by Picard 1.83 to mark PCR duplicates. Genome Analysis Toolkit (GATK) 2.3–9 was then used to remove the duplicates, perform local realignment and map quality score recalibration to produce calibrated bam files for each sample. Multi-sample callings for SNVs were made by GATK. Target regions for variant detection were expanded to 93.9 Mb in total by following the manufacturer's instruction. The annotated VCF files were then filtered using GATK with a stringent filter setting and custom scripts. Variant calls which failed to pass the following filters were eliminated: QUAL < 400 || QD < 2.0 || MQ < 40.0 || FS > 60.0 || HaplotypeScore > 13.0 || GQ <= 60. When genotype is 0/1, 0/2, or 1/2, only SNVs that meet the following conditions were selected: both of the allelic depths >= 8 && difference of the allelic depths within twofold. When genotype is 0/0, 1/1, or 2/2, only SNVs that meet the following conditions were selected: difference of the allelic depths no less than 32-fold, one allelic depth is 1 and the other is no less than 16, or one allelic depth is 0 and the other is no less than 8. Annotations of altered bases were made using SnpEff 3.1 based on GRCh37.69[36]. Custom Perl scripts and C programs are available at http://github.com/glires/genomics/.

Structural mutation analysis. The structural mutation analysis by genome-wide SNP genotyping was performed using Illumina HumanCytoSNP-12 v2.1 DNA Analysis BeadChip Kit. The microarray contains approximately 300,000 SNP markers with an average call frequency of > 99%. Subsequent computational and manual analyses were performed using the Illumina KaryoStudio software. The data have been submitted to the GEO database under accession number GSE54576.

Irradiation. Cells were irradiated by X-ray at 0.87 Gy/min, using MBR-1520R-3 (Hitachi, Tokyo, Japan). Immediately after irradiation, cells were returned to the incubator at 37°C in a humidified atmosphere containing 95% air and 5% CO_2, and incubated until further processing. Cell number was counted with Vi-CELL 1.00. (Beckman Coulter K.K.,Tokyo, Japan).

Teratoma formation. AT-iPS cells were harvested by accutase treatment, collected into tubes, and centrifuged. The same volume of Basement Membrane Matrix (354234, BD Biosciences) was added to the cell suspension. The cells ($>1 \times 10^7$) were subcutaneously inoculated into immuno-deficient, non-obese diabetic (NOD)/severe combined immunodeficiency (SCID) mice (CREA, Tokyo, Japan). After 6 to 10 weeks, the resulting tumors were dissected and fixed with PBS containing 4% paraformaldehyde. Paraffin-embedded tissue was sliced and stained with hematoxylin and eosin (HE). The operation protocols were accepted by the Laboratory Animal Care and the Use Committee of the National Research Institute for Child and Health Development, Tokyo.

Neural differentiation of iPS cells. We employed the standard protocol for neural differentiation of iPS cells[37,38]. Apoptosis was detected by the ApopTag ISOL Dual Fluorescence Apoptosis Detection Kit (DNase Types I & II) APT1000 (Millipore), according to the manufacturer's protocol.

1. Takahashi, K. & Yamanaka, S. Induction of pluripotent stem cells from mouse embryonic and adult fibroblast cultures by defined factors. *Cell* **126**, 663–676 (2006).
2. Yu, J. *et al.* Induced pluripotent stem cell lines derived from human somatic cells. *Science* **318**, 1917–1920 (2007).
3. Hankowski, K. E., Hamazaki, T., Umezawa, A. & Terada, N. Induced pluripotent stem cells as a next-generation biomedical interface. *Lab Invest* **91**, 972–977 (2011).
4. Mavrou, A., Tsangaris, G. T., Roma, E. & Kolialexi, A. The ATM gene and ataxia telangiectasia. *Anticancer Res* **28**, 401–405 (2008).
5. McKinnon, P. J. ATM and ataxia telangiectasia. *EMBO reports* **5**, 772–776 (2004).
6. Kurz, E. U. & Lees-Miller, S. P. DNA damage-induced activation of ATM and ATM-dependent signaling pathways. *DNA Repair (Amst)* **3**, 889–900 (2004).
7. Gatei, M. *et al.* Role for ATM in DNA damage-induced phosphorylation of BRCA1. *Cancer Res* **60**, 3299–3304 (2000).
8. Barlow, C. *et al.* Atm-deficient mice: a paradigm of ataxia telangiectasia. *Cell* **86**, 159–171 (1996).
9. Kinoshita, T. *et al.* Ataxia-telangiectasia mutated (ATM) deficiency decreases reprogramming efficiency and leads to genomic instability in iPS cells. *Biochem Biophys Res Commun* **407**, 321–326 (2011).
10. Kuljis, R. O., Xu, Y., Aguila, M. C. & Baltimore, D. Degeneration of neurons, synapses, and neuropil and glial activation in a murine Atm knockout model of ataxia-telangiectasia. *Proc Natl Acad Sci U S A* **94**, 12688–12693 (1997).
11. Song, H., Chung, S. K. & Xu, Y. Modeling disease in human ESCs using an efficient BAC-based homologous recombination system. *Cell Stem Cell* **6**, 80–89 (2010).
12. Lee, P. *et al.* SMRT compounds abrogate cellular phenotypes of ataxia telangiectasia in neural derivatives of patient-specific hiPSCs. *Nat Commun* **4**, 1824 (2013).
13. Nayler, S. *et al.* Induced pluripotent stem cells from ataxia-telangiectasia recapitulate the cellular phenotype. *Stem Cells Transl Med* **1**, 523–535 (2012).
14. Meek, D. W. The p53 response to DNA damage. *DNA Repair (Amst)* **3**, 1049–1056 (2004).
15. Hong, H. *et al.* Suppression of induced pluripotent stem cell generation by the p53-p21 pathway. *Nature* **460**, 1132–1135 (2009).
16. Kawamura, T. *et al.* Linking the p53 tumour suppressor pathway to somatic cell reprogramming. *Nature* **460**, 1140–1144 (2009).
17. Li, H. *et al.* The Ink4/Arf locus is a barrier for iPS cell reprogramming. *Nature* **460**, 1136–1139 (2009).
18. Marion, R. M. *et al.* A p53-mediated DNA damage response limits reprogramming to ensure iPS cell genomic integrity. *Nature* **460**, 1149–1153 (2009).
19. Utikal, J. *et al.* Immortalization eliminates a roadblock during cellular reprogramming into iPS cells. *Nature* **460**, 1145–1148 (2009).
20. Metcalfe, J. A. *et al.* Accelerated telomere shortening in ataxia telangiectasia. *Nat Genet* **13**, 350–353 (1996).
21. Marion, R. M. *et al.* Telomeres acquire embryonic stem cell characteristics in induced pluripotent stem cells. *Cell Stem Cell* **4**, 141–154 (2009).
22. Davy, P. & Allsopp, R. Balancing out the ends during iPSC nuclear reprogramming. *Cell Stem Cell* **4**, 95–96 (2009).
23. Watson, J. D. Origin of concatemeric T7 DNA. *Nat New Biol* **239**, 197–201 (1972).
24. Harley, C. B., Futcher, A. B. & Greider, C. W. Telomeres shorten during ageing of human fibroblasts. *Nature* **345**, 458–460 (1990).
25. Tchirkov, A. & Lansdorp, P. M. Role of oxidative stress in telomere shortening in cultured fibroblasts from normal individuals and patients with ataxia-telangiectasia. *Hum Mol Genet* **12**, 227–232 (2003).
26. Gore, A. *et al.* Somatic coding mutations in human induced pluripotent stem cells. *Nature* **471**, 63–67 (2011).
27. Ikenaga, M., Midorikawa, M., Abe, J. & Mimaki, T. The sensitivities to radiations and radiomimetic chemicals of cells from patients with ataxia telangiectasia. *Jinrui Idengaku Zasshi* **28**, 1–10 (1983).

28. Makino, H. *et al.* Mesenchymal to embryonic incomplete transition of human cells by chimeric OCT4/3 (POU5F1) with physiological co-activator EWS. *Exp Cell Res* **315**, 2727–2740 (2009).
29. Nishino, K. *et al.* DNA Methylation Dynamics in Human Induced Pluripotent Stem Cells over Time. *PLoS Genet* **7**, e1002085 (2011).
30. Nagata, S. *et al.* Efficient reprogramming of human and mouse primary extra-embryonic cells to pluripotent stem cells. *Genes Cells* **14**, 1395–1404 (2009).
31. Nishino, K. *et al.* Defining hypo-methylated regions of stem cell-specific promoters in human iPS cells derived from extra-embryonic amnions and lung fibroblasts. *PLoS One* **5**, e13017 (2010).
32. Toyoda, M., Kojima, M. & Takeuchi, T. Jumonji is a nuclear protein that participates in the negative regulation of cell growth. *Biochem Biophys Res Commun* **274**, 332–336 (2000).
33. Poon, S. S. & Lansdorp, P. M. Measurements of telomere length on individual chromosomes by image cytometry. *Methods Cell Biol* **64**, 69–96 (2001).
34. Terai, M. *et al.* Investigation of telomere length dynamics in induced pluripotent stem cells using quantitative fluorescence *in situ* hybridization. *Tissue Cell* **45**, 407–413 (2013).
35. Takubo, K. *et al.* Chromosomal instability and telomere lengths of each chromosomal arm measured by Q-FISH in human fibroblast strains prior to replicative senescence. *Mech Ageing Dev* **131**, 614–624 (2010).
36. Cingolani, P. *et al.* A program for annotating and predicting the effects of single nucleotide polymorphisms, SnpEff: SNPs in the genome of Drosophila melanogaster strain w1118; iso-2; iso-3. *Fly (Austin)* **6**, 80–92 (2012).
37. Chambers, S. M. *et al.* Highly efficient neural conversion of human ES and iPS cells by dual inhibition of SMAD signaling. *Nat Biotechnol* **27**, 275–280 (2009).
38. Koch, P., Opitz, T., Steinbeck, J. A., Ladewig, J. & Brüstle, O. A rosette-type, self-renewing human ES cell-derived neural stem cell with potential for in vitro instruction and synaptic integration. *Proc Natl Acad Sci U S A* **106**, 3225–3230 (2009).

Acknowledgments

We would like to express our sincere thanks to M. Yamada for fruitful discussion and critical reading of the manuscript, to H. Abe and H. Kobayashi for providing expert technical assistance, to Dr. C. Ketcham for English editing and proofreading, and to E. Suzuki, Y. Kajiyama, Y. Suehiro, and K. Saito for secretarial work. This research was supported by grants from the Ministry of Education, Culture, Sports, Science, and Technology (MEXT) of Japan; by Ministry of Health, Labor and Welfare (MHLW) Sciences research grants; by a Research Grant on Health Science focusing on Drug Innovation from the Japan Health Science Foundation; by the program for the promotion of Fundamental Studies in Health Science of the Pharmaceuticals and Medical Devices Agency; by the Grant of National Center for Child Health and Development. We acknowledge the International High Cited Research Group (IHCRG #14-104), Deanship of Scientific Research, King Saudi University, Riyadh, Kingdom of Saudi Arabia. AU thanks King Saud University, Riyadh, Kingdom of Saudi Arabia, for the Visiting Professorship.

Author contributions

A.U. designed experiments. Y.F., M.T., K.O., K.Nakamura, K.Nakabayashi, M.Y.I. and K.T. performed experiments. Y.F., M.T., K.O., K.Nakabayashi, M.Y.I., M.N., K.Hata and K.Hanaoka analyzed data. Y.F., M.T., K.O., K.Nakabayashi, S.T., M.Y.I., M.N., K.Hata, AH, and K.Hanaoka contributed reagents, materials and analysis tools. A.M. and A.U. wrote this manuscript.

Additional information

Accession codes The SNP genotyping by SNP array data was uploaded to the ncbi web site (GSE47498: Increased X-ray sensitivity and sustained chromosomal stability in Ataxia Telangiectasia-derived induced pluripotent stem (AT-iPS) cells, GSM1151202: AT1OS cells, GSM1151203: ATiPS-262 cells at passage 17, GSM1151204: ATiPS-263 cells at passage 27, GSM1151205: ATiPS-264 cells at passage 25, GSM1151206: ATiPS-024 cells at passage 25). The exome data was uploaded to the DDBJ Sequence Read Archive (DRP001084).

Supplementary information accompanies this paper at http://www.nature.com/scientificreports

Competing financial interests: The authors declare no competing financial interests.

How to cite this article: Fukawatase, Y. *et al.* Ataxia telangiectasia derived iPS cells show preserved x-ray sensitivity and decreased chromosomal instability. *Sci. Rep.* **4**, 5421; DOI:10.1038/srep05421 (2014).

Regenerative Therapy 1 (2015) 18–29

Contents lists available at ScienceDirect

Regenerative Therapy

journal homepage: http://www.elsevier.com/locate/reth

Original article

Xenogeneic-free defined conditions for derivation and expansion of human embryonic stem cells with mesenchymal stem cells

Hidenori Akutsu [a], Masakazu Machida [a], Seiichi Kanzaki [a], Tohru Sugawara [a], Takashi Ohkura [a], Naoko Nakamura [a], Mayu Yamazaki-Inoue [a], Takumi Miura [a], Mohan C. Vemuri [b], Mahendra S. Rao [c, 1], Kenji Miyado [a], Akihiro Umezawa [a, *]

[a] Department of Reproductive Biology, Center for Regenerative Medicine, National Research Institute for Child Health and Development, 2-10-1 Okura, Setagaya-ku, Tokyo 157-8535, Japan
[b] Thermo Fisher Scientific, 7335 Executive Way, Frederick, MD 21702, USA
[c] Center for Regenerative Medicine, National Institutes of Health, Bethesda, MD 20892, USA

ARTICLE INFO

Article history:
Received 20 July 2014
Received in revised form
17 December 2014
Accepted 28 December 2014

Keywords:
Human embryonic stem cells
Xenogeneic-free medium
Stem cell expansion
Human feeder layer
Mesenchymal stem cells
Gamma irradiation

ABSTRACT

The potential applications of human embryonic stem cells (hESCs) in regenerative medicine and developmental research have made stem cell biology one of the most fascinating and rapidly expanding fields of biomedicine. The first clinical trial of hESCs in humans has begun, and the field of stem cell therapy has just entered a new era. Here, we report seven hESC lines (SEES-1, -2, -3, -4, -5, -6, and -7). Four of them were derived and maintained on irradiated human mesenchymal stem cells (hMSCs) grown in xenogeneic-free defined media and substrate. Xenogeneic-free hMSCs isolated from the subcutaneous tissue of extra fingers from individuals with polydactyly showed appropriate potentials as feeder layers in the pluripotency and growth of hESCs. In this report, we describe a comprehensive characterization of these newly derived SEES cell lines. In addition, we developed a scalable culture system for hESCs having high biological safety by using gamma-irradiated serum replacement and pharmaceutical-grade recombinant basic fibroblast growth factor (bFGF, also known as trafermin). This is first report describing the maintenance of hESC pluripotency using pharmaceutical-grade human recombinant bFGF (trafermin) and gamma-irradiated serum replacement. Our defined medium system provides a path to scalability in Good Manufacturing Practice (GMP) settings for the generation of clinically relevant cell types from pluripotent cells for therapeutic applications.

1. Introduction

Human pluripotent stem cells such as human embryonic stem cells (hESCs) and induced pluripotent stem cells (iPSCs) have remarkable developmental plasticity and therefore possess great potential for drug screening and the development of cellular models to study diseases. hESCs also have potential applications in regenerative medicine as source for cell-based therapy. Since the initial derivation of pluripotent hESCs by Thomson and colleagues in 1998 [1], more than 1000 hESC lines have been established and are now utilized in basic and clinical research worldwide [2]. Several clinical trials using hESC lines approved by the United States Food and Drug Administration (FDA) are currently underway. However, further research is still needed to facilitate the development of safer, reproducible, and scalable culture systems for the generation of hESCs for clinical and industrial purposes.

A key consideration with a cell therapy-compliant culture system, including safe expansion of hESCs, is the choice of culture media, matrix (including feeder layers), and passage procedures. Early hESC culture systems typically include the use of mouse embryonic fibroblast (MEF) feeders or medium conditioned on MEFs in the presence of serum or serum substitutes such as knockout serum replacement [1,3–6]. Human feeders and serum have also been used for hESC culture [7]; however, the use of serum or serum replacement, which contains undefined xenogeneic

* Corresponding author. Tel.: +81 3 5494 7047; fax: +81 3 5494 7048.
E-mail address: umezawa@1985.jukuin.keio.ac.jp (A. Umezawa).
Peer review under responsibility of the Japanese Society for Regenerative Medicine.
[1] Current affiliation: New York Stem Cell Foundation Research Institute, New York, NY 10032, USA.

http://dx.doi.org/10.1016/j.reth.2014.12.004

factors, is still an issue for potential clinical applications of these cells. Transplantation of human cells exposed to animal-derived products can potentially transfer immunogenic sugars such as *N*-glycolylneuraminic acid (Neu5Gc) into the human body and may trigger chronic inflammation and immune reactions [8–10]. Recent studies have identified multiple factors that play a role in sustaining pluripotency and have led to the development of several defined medium systems for hESC culture and derivation [11–13]. Because no reports have described the successful establishment of hESCs in xenogeneic-free (XF) medium, it seems realistic to assume that the most reliable strategies for the establishment of clinical-grade hESCs include the use of a human feeder layer in XF medium, followed by expansion in a feeder-free culture system [14]. There are two strategies for developing hESC culture systems suitable for generation of clinically applicable cells. One approach is to establish XF, defined culture systems especially for future applications, and the other approach is to develop safe conditions for hESC culture systems while continuing to use xenogeneic products. In fact, ongoing clinical trials using hESCs employ conventional hESC culture systems, including mouse feeder layers, under certain conditions [15].

In this study, we developed a novel derivation/cultivation system of hESCs for potential application in translational and clinical research. To completely avoid exposure of hESCs to culture media with animal products, we established an XF culture system containing XF, defined culture medium with inactivated human mesenchymal stem cell (hMSC) feeders. The XF culture system with the hMSC feeder layers proved stable maintenance of self-renewal and pluripotency of newly established hESCs for more than 50 passages. Here, we report the successful derivation of four new hESC lines in this novel XF culture system. Furthermore, we evaluated replacement of a conventional hESC culture system with high-dose gamma-irradiated serum and pharmaceutical-grade recombinant basic fibroblast growth factor (bFGF) to provide insights into the development of a reproducible hESC cultivation system. We examined the pluripotency of SEES cell lines cultivated under the modified conventional culture system. hESCs were able to proliferate under the modified conventional conditions while retaining their pluripotency. Thus, our data provided clinically relevant alternative platforms for clinically and industrially applicable hESC culture systems.

2. Results

Since the first report describing the generation of hESCs by Thomson and coworkers [1], more than 1000 different hESC lines have been established worldwide [2]. Nevertheless, there is still a need for establishment of new hESC lines, particularly from certain HLA types and ethnic groups [16]. In this study, we derived seven new hESC lines using different culture conditions and developed a new hESC culture system using gamma-irradiated KO-SR and pharmaceutical-grade recombinant human bFGF (trafermin). Since our organization name is "Sei-iku" in Japanese, the hESC lines were designated as "SEES (Sei-iku embryonic stem)" in combination with numbers.

2.1. Stable derivation and culture of hESCs under serum replacement conditions

Out of five blastocysts, three hESC lines (SEES-1, SEES-2, and SEES-3) were derived from ICMs on MEF layers using the immunosurgery technique; conventional medium conditions, composed of HUES medium without human plasma protein fraction [4] (Fig. 1A), were used in this derivation. The pluripotency of each of these three SEES cell lines was confirmed by observation of typical morphology and positive immunostaining of stemness markers and differentiated derivatives comprising three embryonic germ layers (Supplemental Figs. 1 and 2). G-banding showed that SEES-1, SEES-2, and SEES-3 cells had normal karyotypes, i.e., 46,XX, 46,XX, and 46,XY, respectively (Supplemental Fig. 1).

2.2. Isolation and characterization of the XF hMSC feeder layer

Primary hMSCs isolated from subcutaneous tissue samples of juvenile donors undergoing surgical procedures for polydactyly were derived and expanded in a complete XF media system that contained an XF supplement, LipoMax, on a humanized substrate, CELLstart (Fig. 2A). Proliferation analysis was performed, and cell morphology was observed by light microscopy to confirm the proliferation assay results. Our data showed that cells grown in MSC-XF medium exhibited high proliferation rates and were self-renewing (Fig. 2B). Flow cytometric characterization was performed to compare surface marker expression characteristics of the

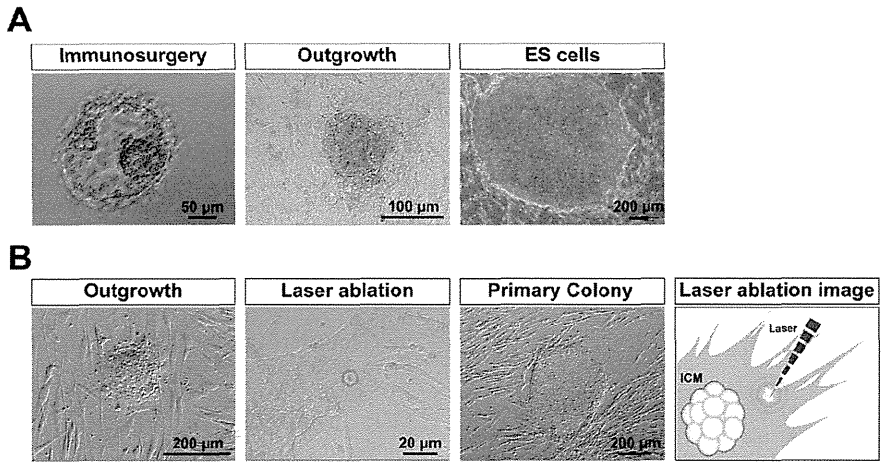

Fig. 1. Derivation of human ES cells by immunosurgery and laser ablation A) The intact inner cell mass (ICM) was isolated from blastocysts by immunosurgery. Cells of the trophectoderm are destroyed by brief exposure to antibodies directed against human cells in tandem with complement activity. Attachment and outgrowth of the ICM grew into an ESC (SEES-1) colony. B) The intact ICM was isolated by laser ablation without any animal products. Outgrowth of the blastocyst grown on human MSC feeder layers. Trophectoderm cells were targeted with multiple pulses of laser ablation. Typical morphology of ESC colonies was readily visible at high magnification. The image shows a schematic of ICM isolation by laser ablation, which is commonly used in artificial reproductive technology (ART).

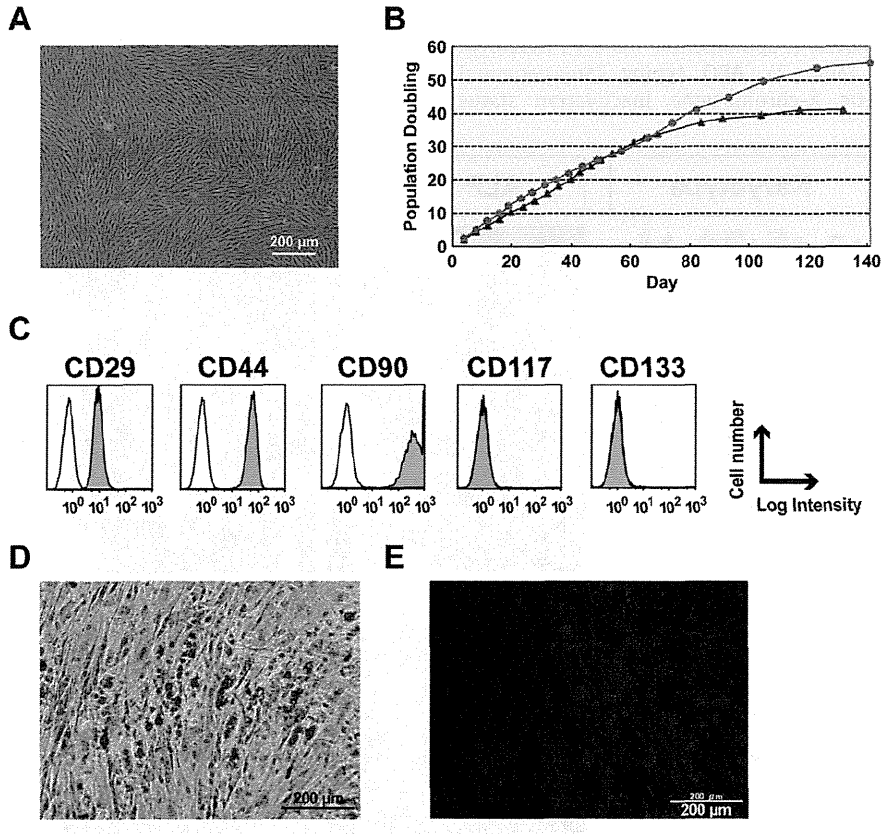

Fig. 2. Isolation and characterization of the xenogeneic-free hMSC feeder layer A) Primary human mesenchymal cells isolated from subcutaneous tissue of the polydactyly were expanded in xenogeneic-free media. B) Cells grew well over PD 30 under xenogeneic-free conditions. Two differentially isolated cell lines (red circle and blue triangle) showed similar cellular proliferation characteristics. C) Mesenchymal markers such as CD29, CD44, and CD90 were observed. D,E) The cells differentiated into adipogenic and osteogenic cells.

cells expanded in the MSC-XF medium. Positive CD29, CD44, and CD90 expression was observed, while CD117 and CD133 were not detected (Fig. 2C). Cells differentiated into both adipogenic and osteogenic cells (Fig. 2D and E). Taken together, our data demonstrated that cells isolated from polydactyly tissues could be classified as MSCs by flow cytometry analysis of their surface markers and evaluation of their multilineage differentiation potential.

2.3. Derivation of new hESC lines in XF culture conditions

To derive an XF hESC line, we first developed an XF culture system using XF hMSC feeder layers. We optimized an XF hESC medium composed of KO-DMEM supplemented with KO-SR XF, amino acids, vitamin C, bFGF, and two other growth factors (IGF1 and heregulin) [17]. All components of the medium were synthetic, recombinant, or of human origin. As a preliminary step, we confirmed the stable cultivation of SEES-1, SEES-2, and SEES-3 cells on XF hMSC feeder layers in XF hESC medium (data not shown). Twelve frozen human embryos were thawed and cultured to the blastocyst stage, and of these, eight blastocysts were used to derive XF hESC lines. Intact blastocysts, without immunosurgery, were plated onto irradiated XF hMSC layers in XF hESC medium. ICM isolation was carried out by exposing TE cells to cell-lethal laser pulses from an XYClone laser system (Fig. 1B). Finally, four XF hESC lines (SEES-4, SEES-5, SEES-6, and SEES-7) were generated and maintained stably (Fig. 3). All of these newly derived XF hESC lines were karyotyped regularly and exhibited a normal diploid karyotype, i.e., 46,XX, 46,XX, 46,XY, and 46,XX, respectively (Fig. 3). To assess the expression of a subset of stemness markers, these cell lines were analyzed by immunocytochemical staining; all XF SEES cell lines expressed the hESC markers NANOG, OCT3/4, SOX2, SSEA4, and TRA1-60 (Fig. 4). We also generated human iPSCs from XF Yub cells by over-expressing three reprogramming factors under hXF culture conditions using XF hESC medium and XF hMSC feeder layers. The XF human iPSCs were stably maintained and expressed the hESC markers such as OCT3/4, NANOG, SSEA4 and TRA1-60 (Supplemental Fig. 3).

2.4. hESCs cultured for prolonged periods in XF culture medium maintained their pluripotency and differentiation characteristics

To evaluate whether the newly derived XF SEES cell lines maintained their pluripotency *in vitro*, we performed EBs assays. EBs differentiated from the cells of SEES-4, SEES-5, SEES-6, and SEES-7 cells expressed markers associated with the three major germ layers: TUJ1 (ectoderm), αSMA (mesoderm), and AFP (endoderm; Fig. 5A). Additionally, in an *in vivo* pluripotency assay, structures from all three germ layers were detected, including neural tissues and pigmented epithelium (ectoderm), cartilage (mesoderm), and gut epithelial tissues (endoderm; Fig. 5B). Sialic acid was released from seven hESCs by acid hydrolysis and quantified by DMB-HPLC. Neu5Gc levels were increased in SEES-1, SEES-2, and SEES-3 cells, while the four XF SEES cell lines (SEES-4, SEES-5, SEES-6, and SEES-7) either did not express Neu5GC at all or had negligible levels of Neu5GC (Supplemental Fig. 4).

The seven SEES cell lines were further characterized by short tandem repeat (STR) analysis (Supplemental Table 1), HLA-DNA typing (Supplemental Table 2), ABO typing (Supplemental Fig. 5), and cytogenetic X-chromosome inactivation status analysis (Supplemental Fig. 6). The distinct features of SEES cell lines could be observed by STR and HLA profiling. SEES-2 and SEES-5 were blood type OO, which is most suitable for cellular transplantation.

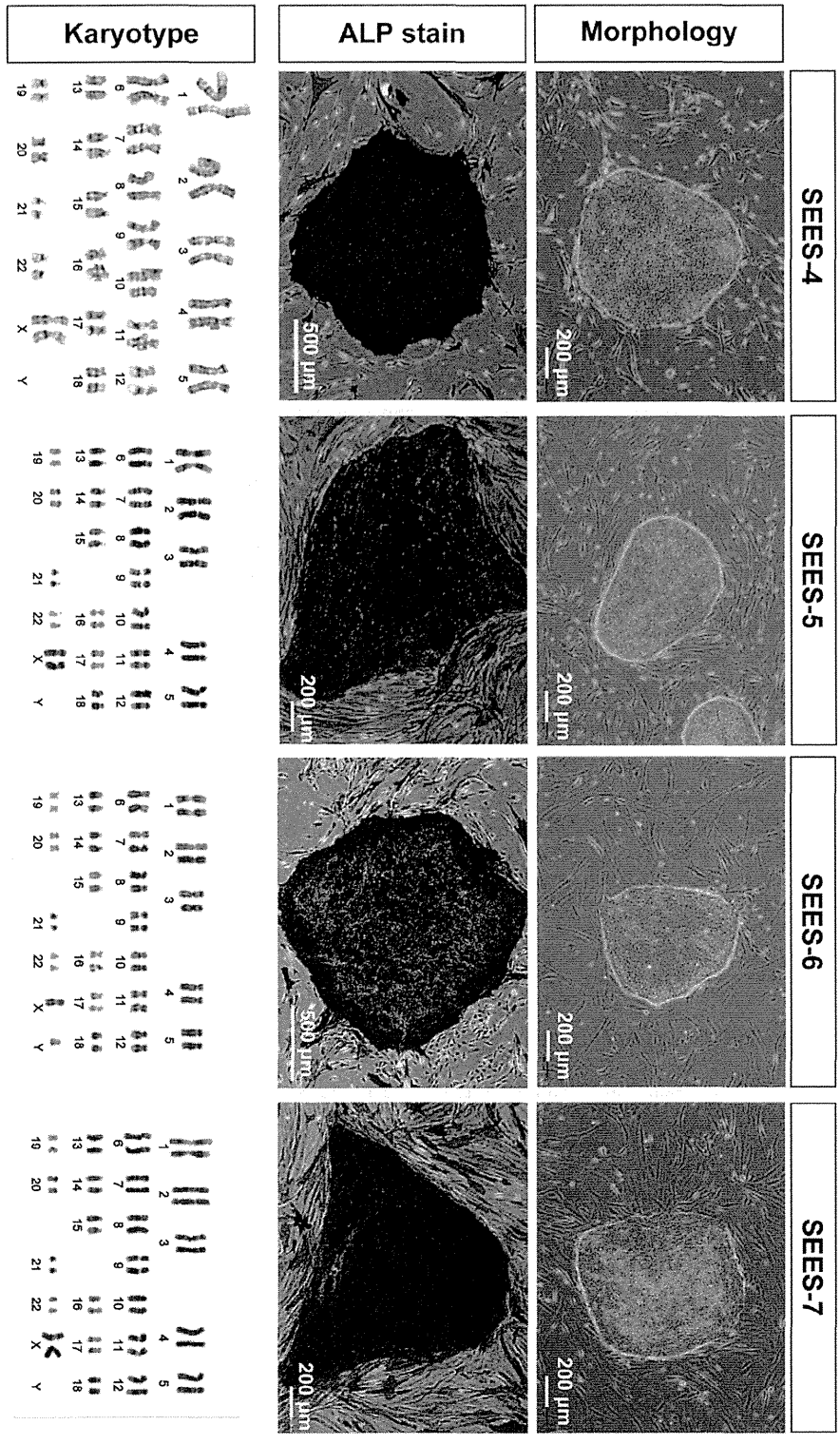

Fig. 3. Derivation of xenogeneic-free hESCs on the hMSC feeder layer Under completely xenogeneic-free conditions, four hESC lines were derived from the inactivated hMSC feeder layer using the laser ablation system. Typical ESC morphology was readily visible. Alkaline phosphatase (ALP) activity was detected in each SEES cell line. Chromosome analysis of SEES-4, SEES-5, SEES-6, and SEES-7 cells showed normal karyotypes: 46,XX, 46,XX, 46,XY, and 46,XX, respectively.

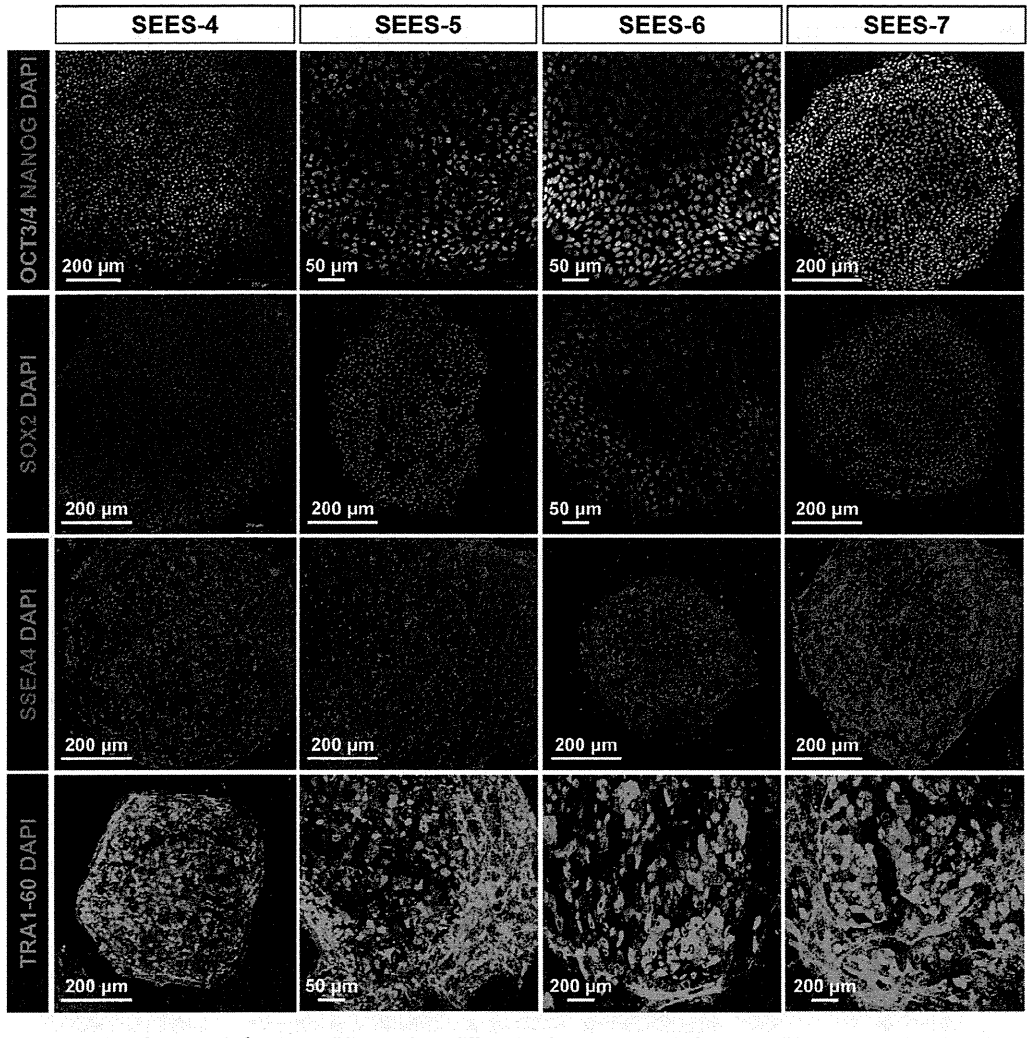

Fig. 4. Pluripotent marker expression of xenogeneic-free SEES cell lines In the undifferentiated state, xenogeneic-free SEES cell lines expressed markers characteristic of pluripotent hESCs, including OCT4, NANOG, SOX2, SSEA4, and TRA1-60. SEES-4: scale bars are 200 μm; SEES-5: scale bars are 50 μm in OCT3/4 and TRA1-60 and 200 μm in SOX2 and SSEA4; SEES-6: scale bars are 50 μm in OCT3/4 and SOX2 and 200 μm in SSEA4; SEES-7: scale bars are 200 μm.

2.5. Stable expansion of SEES cell lines under modified conventional hESC culture conditions

To overcome the shortcomings of conventional approaches, we determined which elements of conventional culture systems were necessary and sufficient for maintaining the pluripotency of hESCs. In our modified conventional hESC culture medium, human recombinant bFGF and KO-SR were replaced by pharmaceutical-grade recombinant human bFGF (trafermin) and high-dose gamma-irradiated KO-SR, respectively. SEES-2 cells were stably maintained on the qualified MEF layer in the modified medium without antibiotics (Fig. 6A). Under these conditions, the colonies expressed multiple pluripotency markers, including OCT3/4, NANOG, SOX2, SSEA4, and TRA1-60, as demonstrated by immunostaining (Fig. 6B). Interestingly, SEES-2 cells could differentiate into derivatives of all three embryonic germ layers *in vitro* and *in vivo*. The EB formation assay showed detection of TUJ1, αSMA, and AFP by immunostaining (Fig. 6C). Additionally, differentiation of the three germ layer *in vivo* was confirmed by teratoma analysis (Fig. 6D), and SEES-2 cells retained normal karyotypes following extensive passaging in culture (Fig. 6E). Under these conditions, cells were able to maintain pluripotency for over 20 passages, as confirmed by positive expression of SSEA4, TRA1-60, and TRA1-80 and absence of SSEA1 expression (Fig. 7). Taken together, our data demonstrated that the modified conventional hESC culture system, based on replacement with high-dose gamma-irradiated KO-SR and trafermin, maintained the pluripotency of hESCs. SEES-1 and SEES-3 also retaining their pluripotency, as shown by morphological analysis and immunostaining (Supplemental Fig. 7). Analysis of the expression of several genes by qRT-PCR showed that hESCs grown under conventional conditions and our modified conditions exhibited highly similar gene expression patterns (Supplemental Fig. 8). Additionally, FISH analysis of SEES cell lines showed that three out of the five SEES cell lines were X-chromosome active.

3. Discussion

Traditional methods for isolating and expanding hESCs include using MEFs as a feeder layer and supplementing medium with FBS replacement. Conventional hESC culture systems are widely used for both basic research and clinical trials under appropriate conditions for ensuring safety [15]. Currently, there are at least two options for further development of hESC cultivation systems for use in regenerative medicine; these methods seek to achieve safe

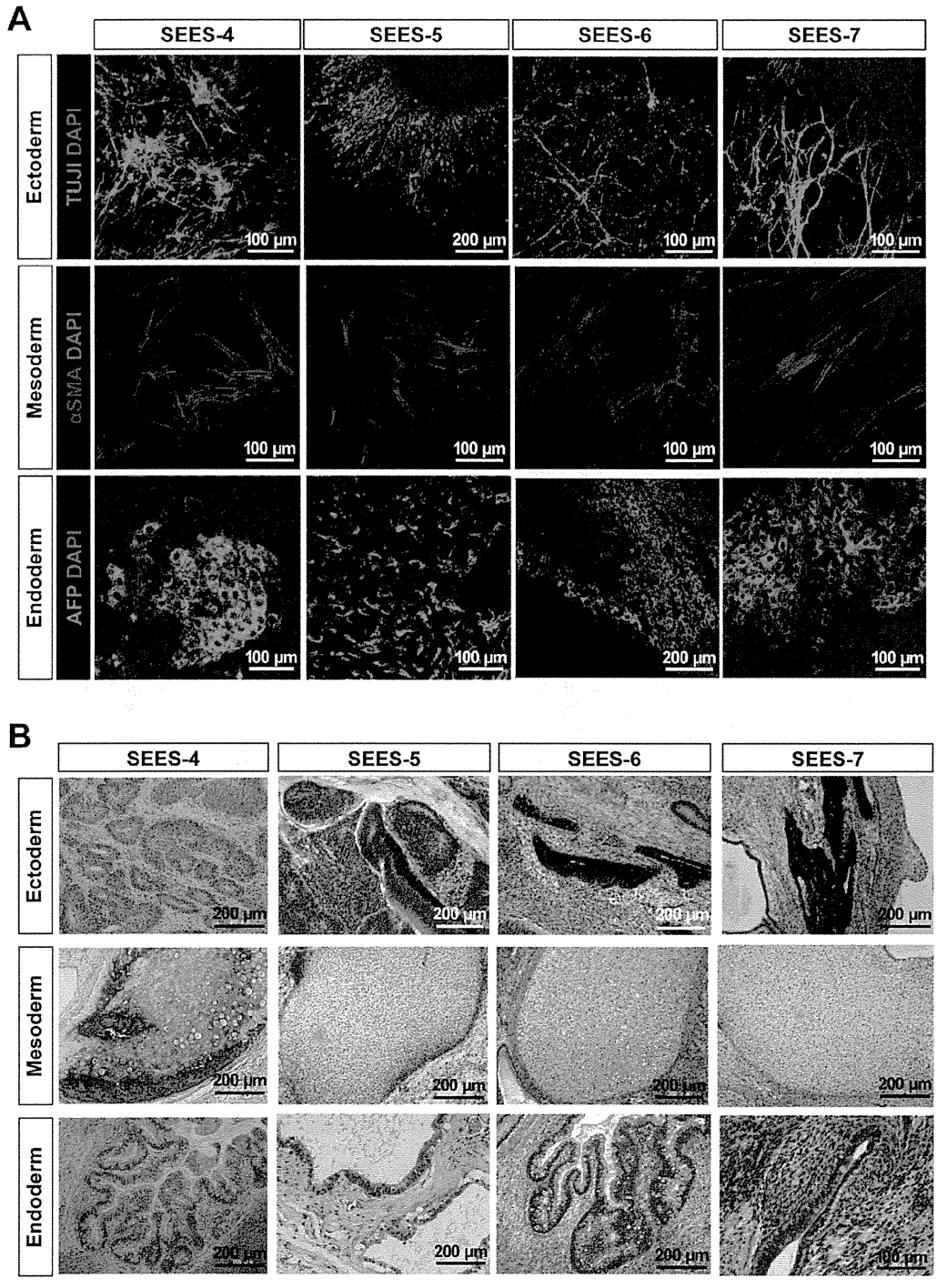

Fig. 5. Differentiation of three germ layers of xenogeneic-free SEES cell lines A) SEES cells differentiated *in vitro* via EBs expressed markers of the primary germ layers. Immunohistochemical analyses of markers of the ectoderm (TUJ1), mesoderm (αSMA), and endoderm (AFP) layers are shown. SEES-4: scale bars are 100 μm; SEES-5: scale bars are 200 μm for TUJ1 and 100 μm for αSMA and AFP; SEES-6: scale bars are 100 μm for TUJ1 and αSMA and 200 μm for AFP; SEES-7: scale bars are 100 μm. B) SEES cells differentiated *in vivo* via teratoma formation. Hematoxylin and eosin staining revealed germ layer derivatives, such as neural tissues, pigmented epithelium (ectoderm), cartilage (mesoderm), and gut epithelial tissues (endoderm). Scale bars are 200 μm.

culture conditions within a stable, conventional hESC cultivation system. Future potential uses of hESCs in clinical and industrial applications will require a reproducible, XF culture system. In this study, we evaluated the replacement of a conventional hESC culture system with high-dose, gamma-irradiated serum and pharmaceutical-grade recombinant bFGF (trafermin) in order to address the reproducibility of hESC cultivation systems. hESCs could be successfully maintained using modified conventional medium supplemented with 35 KGy-irradiated KO-SR and trafermin. Our data provided evidence supporting clinically relevant

alternative platforms of hESC culture for use in clinical and industrial applications. This study also demonstrated the development of a defined, novel, efficient culture system for the derivation of hESCs from blastocyst ICMs and described the expansion and maintenance of hESCs in completely XF conditions on human allogeneic MSC feeder layers. The XF culture system with XF hMSC feeder layers can stably expand several hiPSC lines (data not shown) and successfully allow the derivation of human iPSCs

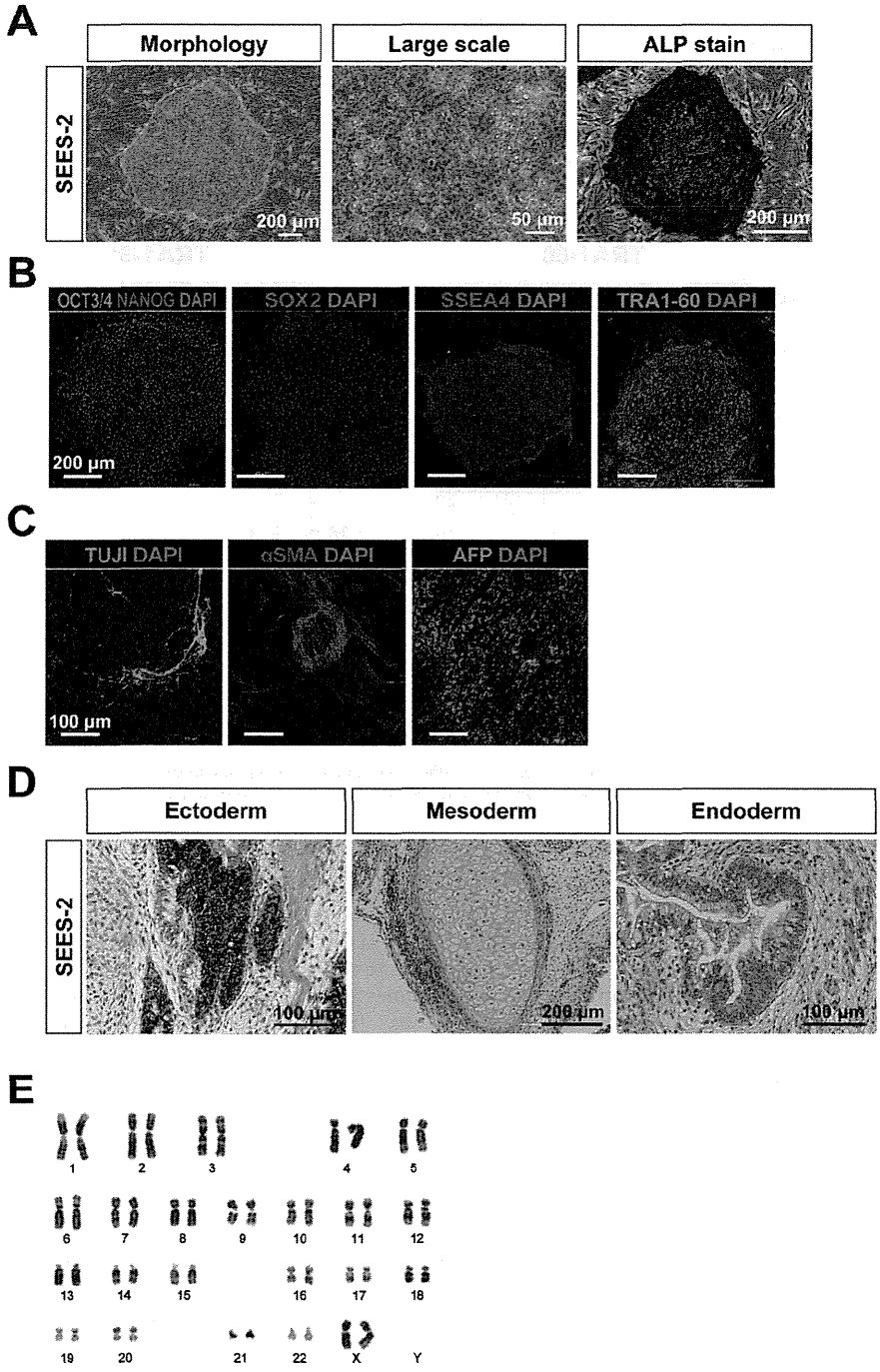

Fig. 6. Characterization of the pluripotency of SEES-2 maintained using a modified conventional hESC culture medium SEES-2 cells were stably maintained over 20 passages on the qualified MEF feeder layer in the modified medium, which contained pharmaceutical-grade recombinant human bFGF (trafermin) and high-dose (35-K) gamma-irradiated KO-SR without antibiotics. A) Typical hESC colony morphology was readily visible. ALP activity was detected. B) SEES-2 cells expressed undifferentiated hESC markers, including OCT4, NANOG, SOX2, SSEA4, and TRA1-60. SEES-2 cells could differentiate into three embryonic germ layers *in vitro* and *in vivo*. Scale bars are 200 μm. C) SEES cells that had been differentiated *in vitro* via EBs expressed markers of the primary germ layers, ectoderm (TUJ1), mesoderm (αSMA), and endoderm (AFP). Scale bars are 100 μm. D) Histological analysis of teratomas containing multidifferentiated tissues derived from SEES-2 cells. Pigmented epithelium (ectoderm), cartilage (mesoderm), and gut epithelial tissues (endoderm). E) Chromosomal analysis of SEES-2 cells cultivated through 16 passages using a modified conventional hESC culture medium showed a normal 46,XX karyotype.

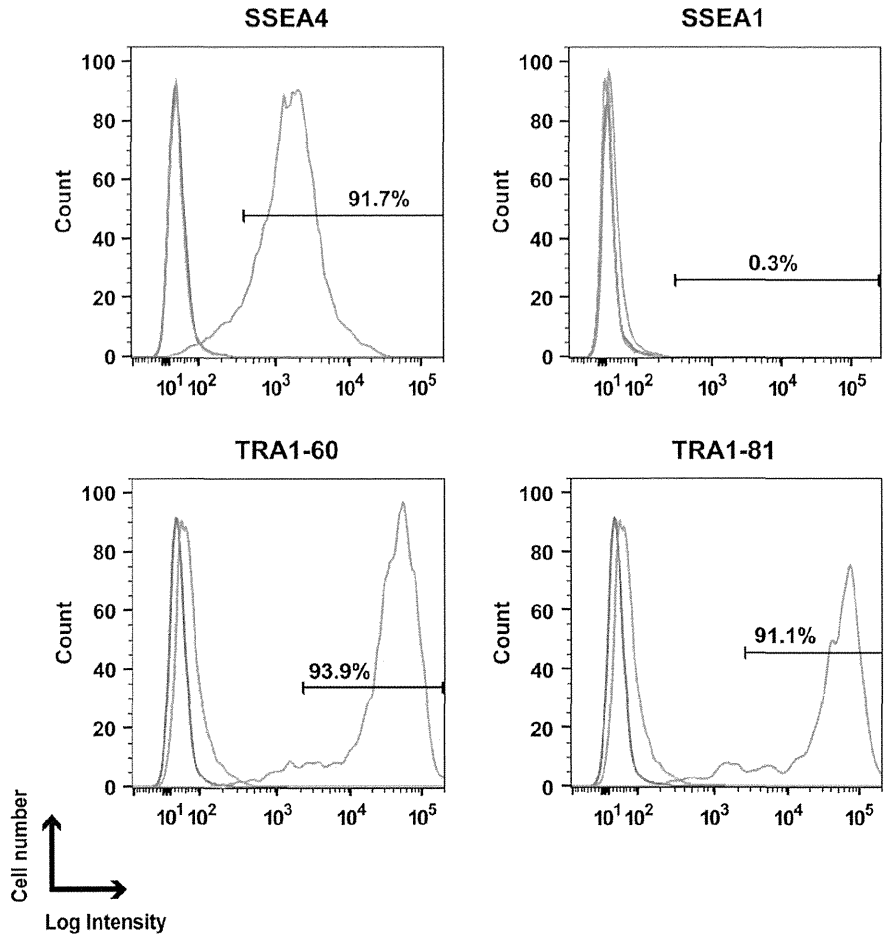

Fig. 7. Expression of pluripotency markers in SEES-2 cells was maintained using a modified conventional hESC culture medium Flow cytometric analysis of hESC-specific marker expression in SEES-2 cells. The isotype control is indicated by the blue line, and the unlabeled sample, which was used as a control, is indicated by the red line. Surface staining is shown by the yellow line for SSEA4, SSEA1, TRA-1-60, and TRA-1-81.

(Supplemental Fig. 3). These conditions are also quite applicable to iPSC derivation and cultivation as well. Importantly, the development of such an XF culture system primarily enables hESCs to culture and expand in conditions that are totally devoid of forming Neu5GC, a sialic acid glycan and xenogeneic antigen that can potentially transform cells to obtain cancer phenotypes [18,19]. In this culture system, we developed and successfully generated completely Neu5GC-free hESC lines. Our four XF hESC lines (SEES-4, SEES-5, SEES-6, and SEES-7) can be also stably cultivated under alternative xenogeneic-free conditions. Nakagawa et al. reported a novel culture system for derivation and expansion of hiPSCs with the recombinant laminin-511 E8 fragment matrices and the xenogeneic-free culture medium (StemFit™) [20]. Four XF SEES cell lines were stably grown using the StemFit™ medium under feeder-free conditions (data not shown). The XF SEES cell lines would be accustomed to being maintained in xenogeneic-free conditions with ease, as these cell lines have been derived and expanded under animal derived components-free conditions.

Pluripotent hESCs are isolated from preimplantation embryos [1] and general characteristics of hESCs include flat morphology, dependence on FGF2 signaling, differentiation into three germ layers *in vitro* and *in vivo*, and pluripotent markers expression [21]. Numerous hESC lines have been derived [3]. It is indicated that many of hESC lines differ in the manner in which they were derived and maintained in culture, and such differences may have significant effects on the characteristics of the cell lines [22,23]. In female hESCs, culture conditions may have significant effects on the X chromosome inactivation status and contribute to the cellular characteristics [24]. Three of five female SEES cell lines showed none of XIST expression in this study. However, it has demonstrated that there are not notable differences in gross hESCs characters including pluripotent markers and differentiation *in vitro* and *in vivo*, despite the significant differences in XIST expression status among SEES 1, 2, 4, 5 and 7. Notably, SEES cell lines are characterized not only the biological properties of human ESCs, also the genomic signatures including ABO blood typing, STR genotyping and HLA isotyping. The distinct properties of the SEES cell lines offer a scalable cell resource for clinical application.

The culture medium we described in this study consisted of a basal culture medium with well-known growth factors that define the maintenance of pluripotency. Since these ingredients are well known and are added to a simple culture medium formulation, the cells derived/expanded in such a system have the potential for reduced contamination, better kinetics of growth, good ability to differentiate into all the three germ layer derivative lineages, maintain a normal karyotype, and, most importantly, will not contribute to tumorigenicity. This defined culture system serves as a better and safer alternative to derive/culture/expand hESCs/iPSCs for larger cell therapy purposes.

4. Materials and methods

4.1. Derivation of hESC lines on inactivated mouse embryonic fibroblast (MEF) feeder cultures

All derivations and cultures of hESC lines in this study were performed in full compliance with the Guidelines on the Derivation and Distribution of Human Embryonic Stem Cells of the Ministry of Education, Culture, Sports, Science and Technology, Japan (Notification No. 156 of 2009), after approval of the Institutional Review Board regarding hESC research at the National Center for Child Health and Development (NCCHD; "Sei-iku" in Japanese title of the affiliation), Japan. Surplus frozen human embryos, donated by consenting couples, were thawed using a Cryotop Safety Thawing Kit (Kitazato BioPharma, Shizuoka, Japan; #VT602) according to the manufacturer's instructions and cultured in BlastAssist System medium (MediCult, Jyllinge, Denmark; #12150010) until they reached the blastocyst stage. The derivation of three hESC lines, i.e., SEES-1, SEES-2, and SEES-3, was performed using modified HUES derivation methods, as described previously [4,5,25]. Briefly, the inner cell mass (ICM) was isolated by immunosurgery by using rabbit antiserum (Rockland Immunochemicals, PA, USA; #109-4139) and guinea pig serum complement (Sigma–Aldrich, MO, USA; #S-1639) and then seeded onto a feeder layer of freshly plated gamma-irradiated MEFs, isolated from ICR embryos at 12.5 gestations and passaged two times before gamma irradiation (30 Gy), in hESC conventional derivation media. The hESC conventional derivation media consisted of Knockout Dulbecco's modified Eagle's medium (KO-DMEM; Life Technologies, CA, USA; #10829-018) supplemented with 20% Knockout Serum Replacement (KO-SR; #10828-028), 2 mM GlutaMAX-I (#35050-079), 0.1 mM nonessential amino acids (NEAAs; #11140-076), 50 U/mL penicillin/50 μg/mL streptomycin (Pen-Strep; #15070-063), 0.055 mM beta-mercaptoethanol (#21985-023), and recombinant human full-length bFGF (#PHG0261) at 10 ng/mL (all reagents were from Life Technologies). Seven to 14 days after ICMs were plated, expanded ICMs were dissected mechanically into small clumps using a finely drawn glass Pasteur pipette and transferred onto a new MEF feeder layer as previously described [4,25]. Secondary colonies were similarly dispersed and plated onto new feeder layers of MEFs until passages 2–4. Cells were then further expanded manually using a Stem Cell Cutting Tool (Vitrolife, Kungsbacka, Sweden; #14601) and Dispase II (Eidia, Ibaraki, Japan; #GD81070).

4.2. hMSCs as feeder layers

4.2.1. Production and culture of hMSCs under XF conditions

To derive and expand hMSC feeder layers under XF conditions, we eliminated the use of media with all animal-derived components during the derivation, propagation, and passaging process in the preparation of new hMSC feeders from human subjects. Parental written informed consent was obtained from all families, and the study was approved by the Institutional Review Board (IRB #88) of the NCCHD. hMSCs were isolated from human dermal tissue samples collected from juvenile donors undergoing surgical procedures for polydactyly in the Division of Orthopedics of the NCCHD. Human dermal tissues were first washed in Dulbecco's phosphate-buffered saline (DPBS) without calcium and magnesium (#14190-250) containing penicillin/streptomycin and then minced into small pieces by using a sterile scalpel in a laminar flow cabinet. The minced tissue was centrifuged and filtered in sequential steps to separate the tissue debris. The isolated cells were then expanded in StemPro MSC SFM XenoFree (MSC-XF; #A10675-01) supplemented with StemPro LipoMax Defined XenoFree Lipid Supplement (#A10850-01) on culture dishes coated with a recombinant humanized matrix (CELLstart CTS; #A10142-01). The isolated cells were expanded in MSC-XF medium with CELLstart using animal-component free TrypLE Select (#12563-011; all reagents from Life Technologies). After approximately 20 days, a confluent monolayer of primary cells was established (passage 0).

4.2.2. Proliferation assay

To assess the proliferative capacity of the isolated cells, primary cultures from two donors were analyzed through 22 serial passages using MSC-XF medium with CELLstart. Cells were counted using a cell viability analyzer (Vi-CELL Cell Viability Analyzer; Beckman Coulter, CA, USA), and cells were subcultured at 10^5 cells/100-mm dish every 4 days for approximately 15 days. At each passage, the population doubling (PD) rate was calculated based on the total cell number using the following formula: $[\log_{10}(N_h) - \log_{10}(N_1)]/\log_{10}(2)$, where N_1 was the number of cells plated and N_h was the number of cells harvested [26]. Growth curves were generated in triplicate using two independent cell lines.

4.2.3. Flow cytometric analysis and in vitro multilineage differentiation assay

Flow cytometric analysis was performed as described previously [27] in order to characterize the cells. Cells were incubated with primary antibodies or isotype-matched control antibodies, followed by immunofluorescence secondary antibody staining and analysis using an EPICS ALTRA analyzer (Beckman Coulter). The following cell surface epitopes were detected with anti-human fluorescein isothiocyanate (FITC)-conjugated or phycoerythrin (PE)-conjugated antibodies: CD29 (Beckman Coulter; #6604105), CD44 (Beckman Coulter; #IM1219), CD90 (BD Pharmingen, CA, USA; #555596), CD117 (Beckman Coulter; #IM1360), and CD133 (Miltenyi Biotec, Bergisch Gladbach, Germany; #130-080-801). The potential of the isolated cells to differentiate into osteogenic and adipogenic lineages was examined according to the manufacturer's instructions. Adipogenesis and osteogenesis were induced by culturing cells in medium from an hMSC Adipogenic BulletKit (Lonza, PA, USA; #PT-3004) or an hMSC Osteogenic BulletKit (Lonza; #PT-3002), respectively. After 8 weeks under differentiation conditions, cells were processed for lineage-specific staining. Oil red staining was used for the detection of accumulated oil droplets in the cytoplasm of cells maintained with adipogenic differentiation media. Alkaline phosphatase activity was used to determine the extent of osteogenesis in cells grown in osteogenic differentiation medium.

4.2.4. Preparation of hMSCs for the feeder layer

At passages 5–20, XF cells were detached from the culture plate with TrypLE Select, washed with MSC-XF medium, and counted. The cells were resuspended in culture medium at a concentration of 1×10^7 cells per tube and then gamma-irradiated with 30 Gy. The irradiated cells were washed in medium and frozen at a concentration of 2×10^6 cells per vial in freezing medium (STEM-CELL-BANKER, ZENOAQ, Fukushima, Japan; #CB043).

4.3. XF hESCs

4.3.1. Derivation and expansion of new hESC lines under XF conditions

The procedure for derivation of XF hESCs was approved by the Institutional Review Board at the NCCHD, and embryos were collected from donors undergoing fertility treatment after obtaining informed consent. Frozen embryos were thawed and cultured to the blastocyst stage under the same methods as used for conventional hESC derivation. Blastocysts without immunosurgery were plated on inactivated XF hMSC feeder layers (Yub-1896 cells)

in XF hESC culture medium composed of 15% Knockout SR Xeno-Free CTS (KO-SR XF; Life Technologies; #12618-013), 85% KO-DMED, 2 mM GlutaMAX-I, 0.1 mM NEAAs, penicillin/streptomycin, 50 μg/mL L-ascorbic acid 2-phosphate (Sigma–Aldrich; #A4544), 10 ng/mL heregulin-1β, recombinant human NRG-beta 1/HRG-beta 1 EGF domain (R&D Systems, MN, USA; #396-HB-050/CF), 200 ng/mL LONG R^3-IGF1, recombinant human insulin-like growth factor-1 (Sigma–Aldrich; #85580C), and recombinant human full-length bFGF (Life Technologies; #PHG0261) at 20 ng/mL. Cells were initially maintained in a drawer-type incubator (IVF CUBE, ASTEC, Fukuoka, Japan; #AR-3100) at 37 °C under the appropriate humidified gas mixture (usually 3%–5% O_2/5% CO_2/90%–92% N_2). Within 7 days after whole blastocysts were plated on the feeder layers, ICMs were isolated by laser-mediated ablation of trophectoderm (TE) cells by using a XYClone laser system (Hamilton Thorne Biosciences, MA, USA) with 80% pulse strength and a pulse length of 300 μs [5]. After 2 weeks, the ICM outgrowth began to resemble morphologically distinct hESCs, and cells could be handpicked and transferred to fresh plates. After the first splitting, new colonies were disaggregated with a recombinant trypsin (Roche Applied Science, Basel, Switzerland; #06369880103) and transferred to fresh mitotically inactivated XF hMSC feeder plates every 5–7 days. Undifferentiated cells, as judged by morphology, were chosen for each further passage. A total of four XF hESC lines were derived and stably maintained (SEES-4, SEES-5, SEES-6, and SEES-7). All four SEES cell lines were maintained in a standard tissue culture incubator at 37 °C under the appropriate humidified gas mixture (3%–5% O_2/5% CO_2/90%–92% N_2) in multigas incubator (Sanyo, Osaka, Japan; #MCO-18M) in a separate culture room to avoid any contamination. SEES cells were cryopreserved using a conventional slow-rate cooling/thawing method with STEM-CELLBANKER. Validation of the cryopreservation by subsequent thawing of individual tubes resulted in efficient recovery of viable, undifferentiated hESCs.

4.3.2. *Immunohistochemical analyses of stem cell and differentiated markers*

Immunohistochemistry was performed as previously described [28,29]. The primary antibodies used for hESCs were specific for Nanog (1:300; ReproCELL, Kanagawa, Japan; #RCAB0003P), Oct3/4 (1:300; Santa Cruz Biotechnology, CA, USA; #sc-5279), Sox2 (1:300; Merck Millipore, Darmstadt, Germany; #AB5603), TRA1-60 (1:300; Merck Millipore; #MAB4360), and SSEA4 (1:300; Merck Millipore; #MAB4304). To assess the differentiation of the three germ layers, the primary antibodies used for embryoid bodies (EBs) were anti-α-fetoprotein (AFP; 1:200; R&D Systems; MAB1368), mouse (ascites) anti-β-tubulin III (TUJ1; 1:1000; Promega; #G712A), and anti-α-smooth muscle actin (αSMA; 1:400; Sigma; #A2547). Cells were fixed in 4% paraformaldehyde and incubated with primary antibodies overnight at 4 °C. Cells were then probed with Alexa Fluor 546 Goat Anti-Mouse IgG- or Alexa Fluor 488 Goat Anti-Rabbit IgG-conjugated secondary antibodies (1:300 each; Life Technologies), counterstained with 1 μg/mL DAPI, for 1 h in the dark at room temperature. After incubation, cells were mounted in Vectashield mounting medium containing 4′, 6-diamidino-2-phenylindole (Vector Laboratories, CA, USA). The labeled cells were visualized using a laser-scanning confocal microscope (LSM 510 META; Carl Zeiss, Oberkochen, Germany). Alkaline phosphatase (ALP) was detected with a Vector Red kit (Vector Laboratories; #SK-5100) according to manufacturer's instructions.

4.3.3. *Flow cytometry analysis of pluripotency markers*

SEES cells cultured in appropriate conditions were stained for 30 min at 4 °C with primary antibodies and immunofluorescence secondary antibodies. Cells were analyzed with a Cytomics FC 500 Cytometer (Beckman Coulter), and data were analyzed with FC 500 CXP Software ver. 2.0 (Beckman Coulter). Antibodies against human SSEA-1 (R&D Systems; #FAB2155C), SSEA4 (R&D Systems; #FAB1435F), TRA1-60 (Merck Millipore; #MAB4360), and TRA1-81 (Merck Millipore; #MAB4381) were used as primary antibodies in hESCs. PE-conjugated anti-mouse IgG antibodies (BD Pharmingen; #555578) and PE-conjugated anti-mouse IgM antibodies (BD Pharmingen; #553472) were used as secondary antibodies. X-Mean, the sum of intensity divided by the total cell number, was automatically calculated and was utilized for our evaluation.

4.3.4. *Differentiation assays in vitro and in vivo*

For induction of differentiation *in vitro*, the cells were dissociated using either StemPro Accutase (Life Technologies; #A11105-01) or TrypLE Select for 5 min at 37 °C, plated into 96-well plates (low attachment surface; Lipidure; NOF Corp., Tokyo, Japan), and cultured in differentiation medium containing KO-DMEM supplemented with 20% fetal bovine serum (FBS), 2 mM GlutaMAX-I, 0.1 mM NEAAs, and penicillin/streptomycin, to generate EBs. After 7 days in suspension, EBs were transferred onto poly-L-ornithine-coated chamber slides and cultured for an additional 10–14 days. The cultures were fixed with 4% paraformaldehyde for 20 min before immunohistochemical analysis.

In vivo pluripotency was assessed by teratoma formation in severe combined immunodeficient nude mice (BALB/cAJcl-nu/nu) purchased from CLEA Japan. A 60-mm plate of undifferentiated hESCs was washed with DPBS, and the cells were harvested with a cell scraper. The cell suspension was collected into a 15-mL conical tube and centrifuged at 1000 rpm for 4 min. The cell pellet was resuspended in hESC culture medium and Matrigel (BD Biosciences, NJ, USA; #356234) to a final total volume of 400 μL. Approximately $2–5 \times 10^6$ cells in 200 μL were injected subcutaneously into the dorsolateral area on both sides. Mice were sacrificed after 8–10 weeks. Tumors were then excised surgically, fixed in 4% paraformaldehyde, embedded in paraffin, sectioned, and stained with hematoxylin and eosin. Hematoxylin and eosin-stained paraffin-embedded sections were histologically examined for the presence of differentiated human tissue derived from all three embryonic germ layers.

The animal use protocol was approved by the Institutional Animal Care and Use Committee of the National Research Institute for Child Health and Development (NRICHD, Permit Number: A2003-002). All experiments with mice were subject to the 3 R consideration (refine, reduce, and replace), and all efforts were made to minimize animal suffering and to reduce the number of animals used.

4.3.5. *Sialic acid analysis*

Sialic acid was released from cell homogenate samples by acid hydrolysis with 0.05 M HCl at 80 °C for 3 h. Sialic acid samples were ultrafiltered using Amicon Ultra-0.5 mL filters (cut-off, 10 kDa; Millipore; #UFC503008), and filtrates were dried in a vacuum concentrator. Sialic acid was derivatized with 1,2-diamino-4,5-methylenedioxybenzene (DMB; Sialic Acid Fluorescence Labeling Kit; Takara Bio, Shiga, Japan) and analyzed by reverse-phase fluorometric HPLC1 using a PALPAK Type R column (Takara Bio). The excitation and emission wavelengths were 310 and 448 nm, respectively. The DMB-derivatized sialic acid was identified by comparing retention times with those of known standards (Glyko Sialic acid reference panel; ProZyme, CA, USA; #GKRP-2503) that were similarly treated. This method can evaluate sialic acids at a minimum concentration of 0.01 nmol/mg protein.

4.3.6. *Karyotype analysis*

Chromosomal G-band analyses were performed at the Nihon Gene Research Laboratories, Sendai, Japan. The chromosomes were

classified according to the International System for Human Cytogenetic Nomenclature. At least 20 metaphase chromosomes were analyzed per cell line.

4.4. Generation of human iPSCs

Human iPSCs were generated from XF Yub-1896 cells by transduction with of a lentiviral vector carrying three reprogramming factors (OCT3/4, SOX2 and KLF4) under XF culture conditions. The vector was a generous gift of Konrad Hochedlinger (Harvard University). XF iPSCs were successfully maintained on inactivated XF hMSC feeder layers in XF hESC culture medium over 20 passages. We confirmed the XF iPSCs expressed pluripotent markers including OCT3/4, NANOG, SSEA4, and TRA1-60.

4.5. Modified conventional hESC cultivation

4.5.1. Production of MEF feeder stock

Pregnant ICR mice were obtained from a breeding colony under specific pathogen-free (SPF) conditions in a barrier room with extensive health monitoring at CLEA Japan (Atsugi facility, Kanagawa, Japan). MEFs were generated from ICR embryos at 12.5 gestations as previously described [5,25] and expanded using MEF feeder sock medium composed of 90% KO-DMEM, 30 KGy gamma-irradiated FBS (HyClone; Thermo Fisher Scientific, MA, USA), and 2 mM GlutaMAX-I without any antibiotics. At passage 2, cells were mitotically inactivated by gamma irradiation (30 Gy) and frozen at a concentration of 4×10^6 cells per vial. To minimize the risk of introducing murine viruses and other pathogens, MEF feeder stock was tested in GMP/GLP studies by Vitology Limited (Glasgow, UK). The specifications and results for the testing of lot MEF-0001 are presented in Supplemental Table 3.

4.5.2. hESC expansion using gamma-irradiated KO-SR and pharmaceutical-grade recombinant human bFGF without antibiotics

To develop a safer culture system for clinical application of hESCs, we replaced KO-SR and recombinant human full-length bFGF with pharmaceutical recombinant human bFGF and high-dose gamma–irradiated KO-SR. Frozen KO-SR products ware gamma irradiated at 35 KGy (KOGA ISOTOPE, Ltd., Shiga, Japan). Pharmaceutical-grade recombinant human bFGF (generic name: trafermin), supplied by Kaken Pharmaceutical (Tokyo, Japan) as Fiblast Spray, which is prepared using the powdered form of trafermin, was applied for hESC culture. hESC lines were cultivated in a modified conventional culture medium composed of 20% gamma-irradiated KO-SR, 80% KO-DMEM, 2 mM GlutaMAX-I, 0.1 mM NEAAs, and 50 ng/mL trafermin without any antibiotics on plates coated with 0.1% type I collagen (Nippon Ham, Ibaraki, Japan; #307-31611) and a mitotically inactivated layer of MEFs.

Competing financial interests

The authors declare no competing financial interests.

Acknowledgments

We are grateful to Hideki Tsumura and the staff of the Animal Care Facility at NRICHD for mouse husbandry. We thank Kaken Pharmaceutical for providing us with the trafermin used in this study. We thank Kahori Minami and Nobuyuki Watanabe for technical assistance and Tomoyuki Kawasaki for help with editing the figures. The authors would like to thank members of the Umezawa laboratory for helpful suggestions.

This research was supported by grants from the Ministry of Education, Culture, Sports, Science, and Technology (MEXT) of Japan; by Ministry of Health, Labor and Welfare (MHLW) Sciences research grants; by a Research Grant on Health Science focusing on Drug Innovation from the Japan Health Science Foundation; by the program for the promotion of Fundamental Studies in Health Science of the Pharmaceuticals and Medical Devices Agency; by the Grant of National Center for Child Health and Development; by the Takeda Science Foundation to HA and AU. This research was also by a grant from JST-CREST to HA. AU acknowledges the International High Cited Research Group (IHCRG #14-104), Deanship of Scientific Research, King Saudi University, Riyadh, Kingdom of Saudi Arabia. AU also thanks King Saud University, Riyadh, Kingdom of Saudi Arabia, for the Visiting Professorship. The funders had no control over the study design, data collection and analysis, decision to publish, or preparation of the manuscript.

Appendix A. Supplementary data

Supplementary data related to this article can be found at http://dx.doi.org/10.1016/j.reth.2014.12.004.

References

[1] Thomson JA, Itskovitz-Eldor J, Shapiro SS, Waknitz MA, Swiergiel JJ, Marshall VS, et al. Embryonic stem cell lines derived from human blastocysts. Science 1998;282:1145–7.
[2] Schuldt BM, Guhr A, Lenz M, Kobold S, MacArthur BD, Schuppert A, et al. Power-laws and the use of pluripotent stem cell lines. PLoS One 2013;8:e52068.
[3] Amit M, Carpenter MK, Inokuma MS, Chiu CP, Harris CP, Waknitz MA, et al. Clonally derived human embryonic stem cell lines maintain pluripotency and proliferative potential for prolonged periods of culture. Dev Biol 2000;227:271–8.
[4] Cowan CA, Klimanskaya I, McMahon J, Atienza J, Witmyer J, Zucker JP, et al. Derivation of embryonic stem-cell lines from human blastocysts. N Engl J Med 2004;350:1353–6.
[5] Chen AE, Egli D, Niakan K, Deng J, Akutsu H, Yamaki M, et al. Optimal timing of inner cell mass isolation increases the efficiency of human embryonic stem cell derivation and allows generation of sibling cell lines. Cell Stem Cell 2009;4:103–6.
[6] Xu C, Inokuma MS, Denham J, Golds K, Kundu P, Gold JD, et al. Feeder-free growth of undifferentiated human embryonic stem cells. Nat Biotechnol 2001;19:971–4.
[7] Richards M, Fong CY, Chan WK, Wong PC, Bongso A. Human feeders support prolonged undifferentiated growth of human inner cell masses and embryonic stem cells. Nat Biotechnol 2002;20:933–6.
[8] Martin MJ, Muotri A, Gage F, Varki A. Human embryonic stem cells express an immunogenic nonhuman sialic acid. Nat Med 2005;11:228–32.
[9] Pham T, Gregg CJ, Karp F, Chow R, Padler-Karavani V, Cao H, et al. Evidence for a novel human-specific xeno-auto-antibody response against vascular endothelium. Blood 2009;114:5225–35.
[10] Varki A. Colloquium paper: uniquely human evolution of sialic acid genetics and biology. Proc Natl Acad Sci U S A 2010;107(Suppl. 2):8939–46.
[11] Ludwig TE, Levenstein ME, Jones JM, Berggren WT, Mitchen ER, Frane JL, et al. Derivation of human embryonic stem cells in defined conditions. Nat Biotechnol 2006;24:185–7.
[12] Lu J, Hou R, Booth CJ, Yang SH, Snyder M. Defined culture conditions of human embryonic stem cells. Proc Natl Acad Sci U S A 2006;103:5688–93.
[13] Yao S, Chen S, Clark J, Hao E, Beattie GM, Hayek A, et al. Long-term self-renewal and directed differentiation of human embryonic stem cells in chemically defined conditions. Proc Natl Acad Sci U S A 2006;103:6907–12.
[14] Hasegawa K, Pomeroy JE, Pera MF. Current technology for the derivation of pluripotent stem cell lines from human embryos. Cell Stem Cell 2010;6:521–31.
[15] Schwartz SD, Hubschman JP, Heilwell G, Franco-Cardenas V, Pan CK, Ostrick RM, et al. Embryonic stem cell trials for macular degeneration: a preliminary report. Lancet 2012;379:713–20.
[16] Fraga AM, Souza de Araújo E, Stabellini R, Vergani N, Pereira LV. A survey of parameters involved in the establishment of new lines of human embryonic stem cells. Stem Cell Rev 2011;7:775–81.
[17] Wang L, Schulz TC, Sherrer ES, Dauphin DS, Shin S, Nelson AM, et al. Self-renewal of human embryonic stem cells requires insulin-like growth factor-1 receptor and ERBB2 receptor signaling. Blood 2007;110:4111–9.
[18] Hedlund M, Padler-Karavani V, Varki NM, Varki A. Evidence for a human-specific mechanism for diet and antibody-mediated inflammation in carcinoma progression. Proc Natl Acad Sci U S A 2008;105:18936–41.
[19] Pearce OM, Läubli H, Verhagen A, Secrest P, Zhang J, Varki NM, et al. Inverse hormesis of cancer growth mediated by narrow ranges of tumor-directed antibodies. Proc Natl Acad Sci U S A 2014;111:5998–6003.

[20] Nakagawa M, Taniguchi Y, Senda S, Takizawa N, Ichisaka T, Asano K, et al. A novel efficient feeder-free culture system for the derivation of human induced pluripotent stem cells. Sci Rep 2014;4:3594.
[21] Hanna JH, Saha K, Jaenisch R. Pluripotency and cellular reprogramming: facts, hypotheses, unresolved issues. Cell 2010;143:508–25.
[22] Hoffman LM, Carpenter MK. Characterization and culture of human embryonic stem cells. Nat Biotechnol 2005;23:699–708.
[23] Hoffman LM, Hall L, Batten JL, Young H, Pardasani D, Baetge EE, et al. X-inactivation status varies in human embryonic stem cell lines. Stem Cells 2005;23:1468–78.
[24] Nguyen HT, Geens M, Spits C. Genetic and epigenetic instability in human pluripotent stem cells. Hum Reprod Update 2013;19:187–205.
[25] Akutsu H, Cowan CA, Melton D. Human embryonic stem cells. Methods Enzymol 2006;418:78–92.
[26] Escobedo-Lucea C, Bellver C, Gandia C, Sanz-Garcia A, Esteban FJ, Mirabet V, et al. A xenogeneic-free protocol for isolation and expansion of human adipose stem cells for clinical uses. PLoS One 2013;8:e67870.
[27] Cui CH, Miyoshi S, Tsuji H, Makino H, Kanzaki S, Kami D, et al. Dystrophin conferral using human endothelium expressing HLA-E in the non-immunosuppressive murine model of Duchenne muscular dystrophy. Hum Mol Genet 2011;20:235–44.
[28] Nagata S, Toyoda M, Yamaguchi S, Hirano K, Makino H, Nishino K, et al. Efficient reprogramming of human and mouse primary extra-embryonic cells to pluripotent stem cells. Genes Cells 2009;14:1395–404.
[29] Makino H, Toyoda M, Matsumoto K, Saito H, Nishino K, Fukawatase Y, et al. Mesenchymal to embryonic incomplete transition of human cells by chimeric OCT4/3 (POU5F1) with physiological co-activator EWS. Exp Cell Res 2009;315:2727–40.

References in supplemental figures

[1] Hosoi E. Biological and clinical aspects of ABO blood group system. J Med Invest 2008;55:174–82 (For Supplemental Figure S1).
[2] Ota M, Fukushima H, Kulski JK, Inoko H. Single nucleotide polymorphism detection by polymerase chain reaction-restriction fragment length polymorphism. Nat Protoc 2007;2:2857–64 (For Supplemental Figure S2).
[3] Muro T, Fujihara J, Imamura S, Nakamura H, Kimura-Kataoka K, Toga T, et al. Determination of ABO genotypes by real-time PCR using allele-specific primers. Leg Med Tokyo 2012;14:47–50 (For Supplemental Figure S3).

Neuroscience Research xxx (2015) xxx–xxx

Contents lists available at ScienceDirect

Neuroscience Research

journal homepage: www.elsevier.com/locate/neures

Magnetic resonance monitoring of superparamagnetic iron oxide (SPIO)-labeled stem cells transplanted into the inner ear

Yukiko Watada[a], Daisuke Yamashita[a,b], Masashi Toyoda[c,d], Kohei Tsuchiya[c], Naoko Hida[c,d], Akihiro Tanimoto[e], Kaoru Ogawa[a], Sho Kanzaki[a,*], Akihiro Umezawa[c]

[a] Department of Otorhinolaryngology, Head and Neck Surgery, Keio University School of Medicine, Tokyo, Japan
[b] Department of Otorhinolaryngology, Head and Neck Surgery, Kobe University Hospital, Kobe, Japan
[c] Department of Department of Reproductive Biology, National Institute for Child Health and Development, Tokyo, Japan
[d] Research Team for Vascular Medicine, Tokyo, Metropolitan Institute of Gerontology, Tokyo, Japan
[e] Department of Diagnostic Radiology, Keio University School of Medicine, Tokyo, Japan

ARTICLE INFO

Article history:
Received 9 September 2013
Received in revised form 13 January 2015
Accepted 21 January 2015
Available online xxx

Keywords:
Cochlea
Transplantation
Mesenchymal stem cells
Superparamagnetic iron oxide
Magnetic resonance imaging
Guinea pigs

ABSTRACT

In the field of regenerative medicine, cell transplantation or cell-based therapies for inner ear defects are considered to be promising candidates for a therapeutic strategy. In this paper, we report on a study that examined the use of magnetic resonance imaging (MRI) to monitor stem cells transplanted into the cochlea labeled with superparamagnetic iron oxide (SPIO), a contrast agent commonly used with MRI. First, we demonstrated *in vitro* that stem cells efficiently took up SPIO particles. This was confirmed by Prussian blue staining and TEM. In MRI studies, T2 relaxation times of SPIO-labeled cells decreased in a dose-dependent manner. Next, we transplanted SPIO-labeled cells directly into the cochlea *in vivo* and then performed MRI 1 h, 2 weeks, and 4 weeks after transplantation. The images were evaluated objectively by measuring signal intensity (SI). SI within the ears receiving transplants was significantly lower ($P<0.05$) than that of control sides at the 1-h assessment. This novel method will be helpful for evaluating stem cell therapies, which represents a new strategy for inner ear regeneration. To the best of our knowledge, this study is the first to demonstrate that local transplantation of labeled stem cells into the inner ear can be visualized *in vivo via* MRI.

1. Introduction

In the field of regenerative therapy for inner ear damage, cell transplantation and cell-based therapy show promise as therapeutic strategies for treating sensorineural hearing loss (SNHL) (Groves, 2010). The utility of stem cell transplantation has already been demonstrated in noise-exposed mouse and guinea pig models of damage (Cotanche and Kaiser, 2010), and in a rat model with lateral wall fibrocyte injury (Kamiya et al., 2007). As with other kinds of stem cells, mesenchymal stem cells (MSCs) display self-renewal and multipotentiality, which make them ideal candidates for transplantation into the inner ear (Pittenger et al., 1999; Jeon et al., 2007; Geraerts and Verfaillie, 2009). When MSCs are transplanted into postnatal animals, they have the ability to graft and differentiate into several tissue-specific cell types in response to environmental cues provided by different organs (Jiang et al., 2002). MSCs are relatively easy to obtain and culture, and they proliferate prodigiously *in vitro*. In addition, most serious ethical and technical problems associated with embryonic stem cells (ES cells) are absent with MSCs (Meyer et al., 2010). The potential therapeutic uses of MSC transplantation, therefore, hold great promise for future cell-based therapies.

Cells transplanted into the inner ear are usually not detectable in living animals. Because the inner ear is encased by temporal bone, it is extremely difficult to observe what occurs inside the ear in living animals. Thus, a method for monitoring cells transplanted into the inner ear would be invaluable. Recently, magnetic resonance imaging (MRI) has proven to be an effective tool for *in vivo* visualization of transplanted cells, with nearly light microscopic resolution. However, in order to detect transplanted cells with MRI, they need to be labeled with a cell-specific agent. For cell labeling, we chose superparamagnetic iron oxide (SPIO), a contrast agent commonly used with MRI. SPIO is an iron oxide nanoparticle solution with a total iron content of 24.9 mg/mL. SPIO already has been

* Corresponding author at: Department of Otorhinolaryngology, Head and Neck Surgery, Keio University School of Medicine, 35 Shinanomachi, Shinjuku, Tokyo 160-8582, Japan. Tel.: +81 3 3353 1211; fax: +81 3 3353 1211.
E-mail address: skan@a7.keio.jp (S. Kanzaki).

http://dx.doi.org/10.1016/j.neures.2015.01.010
0168-0102/

approved for clinical use in liver imaging. Cell labeling techniques with SPIO have been used as a diagnostic modality to track transplanted cells in living tissues (Bulte and Kraitchman, 2004; Arbab et al., 2005; Hsiao et al., 2007; Cicchetti et al., 2007; Farrell et al., 2008). In different types of models, SPIO-labeled cells transplanted *via* a transportal approach or *via* local administration were monitored by MRI scanning. For instance, labeling methods using SPIO have been used in heart (Amsalem et al., 2007; Peng et al., 2011); spinal cord (Sykova and Jendelova, 2007); and brain (Guo et al., 2011). In the present study, we labeled MSCs with SPIO *in vitro*, transplanted them into the inner ear, and monitored labeled cells in the cochleae of living animals using MRI.

2. Materials and methods

2.1. MSC isolation and culture

After obtaining signed informed consent, we harvested bone marrow cells from a 91-year-old male, as described previously (Takeda et al., 2004). Bone marrow stromal cells were obtained from a human donor and subcloned by limiting dilution. One of the cell types isolated was designated H4-1 (Takeda et al., 2004). H4-1 cells were cultured in MSC growth medium (MSCGM) at 37 °C under a humidified 5% CO_2 atmosphere. UET-13 cells, H4-1 cells having an extended life span due to retroviral transduction (Mori et al., 2005), were cultured in Dulbecco's Modified Eagle's Medium (DMEM) with 10% fetal bovine serum (FBS) at 37 °C under a humidified 5% CO_2 atmosphere. In this study, we used H4-1 cells for the *in vitro* study (see Sections 2.3 and 2.4) and UET-13 cells for the *in vivo* study (see Sections 2.5, 2.6 and 2.7).

2.2. Labeling MSCs with SPIO

The contrast agent SPIO (Resovist®; Bayer Schering Pharma, Osaka, Japan) consists of a colloidal solution of iron oxide nanoparticles coated with carboxydextran, generically called Ferucarbotran. Ferucarbotran was diluted with cell culture medium, and cells were incubated with 0.1% Ferucarbotran medium (27.9 μg Fe/mL) for 24 h. After 24 h, the contrast agent was washed out with phosphate-buffered saline, and the cells were detached by incubating them with 0.25% trypsin. The cells were then washed three times to remove excess contrast agent prior to the assays.

2.3. Prussian blue staining and electron microscopic observations

To visualize the iron-labeled cells, we used standard Prussian blue staining. Briefly, cells adhering to the bottom of plastic culture dishes were fixed with 4% paraformaldehyde, washed, incubated for 30 min with Perls agent in hydrochloric acid, and then washed, and counterstained with Fast Red solution. Also, they were examined by transmission electron microscopy (TEM). Beforehand, they were fixed in 2.5% glutaraldehyde, postfixed in 1% osmium tetroxide, dehydrated, and embedded in resin. Ultrathin sections (70–90 nm) were cut and stained with 2% uranyl acetate and Reynold's lead citrate before being examined with a JEM-1200 EX microscope (JOEL) at 80 kV.

2.4. MR relaxometry

Agar gel phantoms doped with graded concentrations of labeled or unlabeled cells were prepared for measurement. Cell suspensions were concentrated twice to a final concentration ranging from 1×10^2 cells/mL to 1×10^7 cells/mL. These were mixed with the same volume of 2% molten agar gel, and then the solution was stirred in a cold water bath until it solidified. The relaxivities, R2 (spin-spin relaxation rate, 1/T2), were measured at 0.47 T using a PC120 Minispec (Bruker Optics, Tsukuba, Japan). MR images of each phantom were obtained a 1.5 T (GE Healthcare, Buckinghamshire, UK) superconducting magnet with T2-weighted (2000/30) spin-echo sequences.

2.5. Animals and surgery

We used seven 4-week-old male Hartley guinea pigs with a normal Preyer's reflex (body weight: 268.4 ± 15.4 g). The animals were purchased from Japan SLC (Hamamatsu, Japan) and were bred at the Laboratory Animal Center, School of Medicine, Keio University under specific pathogen-free (SPF) conditions. All animal experiments were performed in accordance with the guidelines of the Keio University Committee for the Use and Care of Animals. Keio University is fully accredited by the Association for Assessment and Accreditation of Laboratory Animal Care International. Before transplantation, we prepared suspensions of SPIO-labeled MSCs (1×10^7 cells in 200 μl of 10% FBS in DMEM). All animal subjects were anesthetized with intramuscular injections of xylazine (10 mg/kg) and ketamine (40 mg/kg). A skin incision was made posterior to the left pinna near the external auditory meatus after local administration of lidocaine (1%). After the otic bulla was exposed, a small hole was made on the otic bulla. The cochleostomy was made in the lateral wall of the lower basal turn near the round window at the level of the scala tympani. To inject, we used a 100-μl Hamilton syringe with an attached vinyl cannula and fine polyamide tip. Then we injected SPIO-labeled cells directly into the scala tympani; the number of the injected cells was 5×10^3 to 5×10^4/μl × 10 μl. After injection, the cochleostomy site was sealed with a muscle plug and the skin wound was closed with sutures. After cell transplantation, animals were immunosuppressed by administering oral FK506 (1 mg/kg per day) for the 4-week duration of the study. All subjects but one received SPIO-labeled MSC transplants in the left ear. The remaining one subject received the same amount of saline vehicle in the right cochlea; this animal served as a sham. The right ears of MSC-transplanted animals received saline injections; these were untreated controls.

2.6. In vivo MR imaging

One hour, 2 weeks, and 4 weeks after transplantation, we performed MRI experiments using a 1.5 T clinical unit (1.5 T Sigma EXCITE XI, General Electric Medical Systems, Milwaukee, WI, USA). All guinea pigs were anesthetized with intramuscular injections of xylazine (10 mg/kg) and ketamine (40 mg/kg), and immobilized in the prone position. The guinea pigs were sacrificed under deeply anesthetized conditions either 1 h ($n = 3$) or 4 weeks ($n = 4$) after MRI. Scanning was performed using a balanced steady-state free precession (SSFP) sequence (3D-FIESTA) in the coronal plane with the following imaging parameters: TR/TE = 6.7/2.1 ms; flip angle = 25°; field of view (FOV) = 10 × 10/*Z*; matrix number = 256 × 256; slice thickness = 0.6 mm; and number of excitation = 110. We reconstructed serial images using freely available DICOM software (OsiriX) and measured signal intensity (SI) values of these images in order to compare SI levels over time. We measured the SI value of each 1 mm^2 area around the basal turn of the cochlea and the submandibular muscle; we also measured the SI background noise. Next, we calculated contrast-to-noise ratios (CNR) in order to offset differences between images. CNR was calculated as follows: $SIE - SIM/SIN$, where SIE = SI of ear; SIM = SI of muscle; and SIN = SI of background noise. For statistical analyses, we used Student's *t* tests. Differences with $P < 0.05$ was considered significant.

Please cite this article in press as: Watada, Y., et al., Magnetic resonance monitoring of superparamagnetic iron oxide (SPIO)-labeled stem cells transplanted into the inner ear. Neurosci. Res. (2015), http://dx.doi.org/10.1016/j.neures.2015.01.010

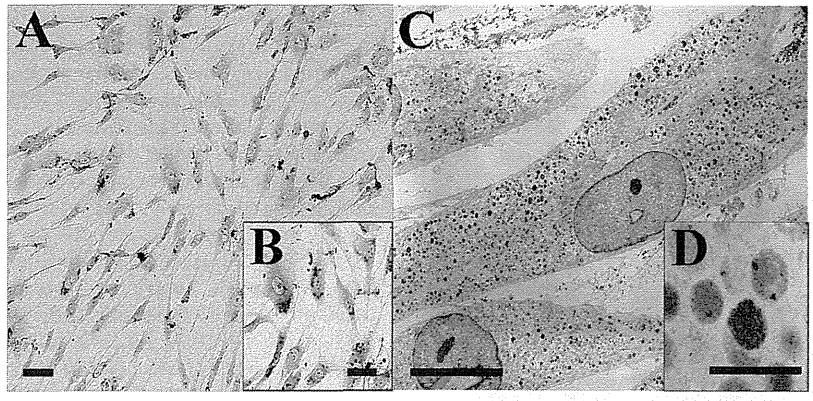

Fig. 1. Prussian blue staining. (A) Prussian blue staining of SPIO-labeled MSCs. (B) Several blue granules were evident in the cytoplasm around the nucleus. (C) Transmission electron micrograph of SPIO-labeled MSCs revealed numerous vesicles in the cytoplasm that were filled with electron-dense magnetic iron particles (D). Scale bars: A, 10 μm; B, 5 μm; C, 5 μm; D, 1 μm. (For interpretation of the references to color in this figure legend, the reader is referred to the web version of this article.)

2.7. Histological analysis

At each time point, the guinea pigs were first deeply anesthetized and then decapitated. After decapitation, both cochleae were removed and immediately placed in 0.01 mol/L phosphate buffer (pH 7.4) Then these were immersed in a fixative consisting of freshly depolymerized 4% paraformaldehyde in 0.1 mol/L phosphate buffer (pH 7.4). Small openings were made in the round window, oval window, and the apex of the cochlea. After overnight fixation, the temporal bones were decalcified by immersion in 5% sucrose, 5% ethylenediaminetetraacetic acid (EDTA; pH 7.4) at 4 °C for 14 days on a stir plate. The specimens were dehydrated through graded concentrations of alcohol, embedded in paraffin blocks, and sectioned into 10 μm-thick slices.

The sections were stained with hematoxylin and eosin (H&E) as generally described and with Prussian blue as described below. For Prussian blue staining, after deparaffinization and rehydration, tissue slices mounted on glass slides were stained in Prussian blue working solution for 2–3 min. The sections were washed in distilled water three times, then quickly dehydrated first with 95% alcohol, then 100% alcohol (2×). (The slides were dipped 10 times in each alcohol solution since the stain fades quickly in alcohol). The sections were cleared in xylene two times for 3 min each.

For Iba-1 staining, the sections were incubated in 0.3% H_2O_2 in methanol prior to primary antibody incubation to block nonspecific peroxidase staining and to avoid tissue destruction. The sections were then incubated in primary antibody against Iba-1 (ABCAM #AB5076) at a dilution of 1:100 for 1 h at room temperature. After rinsing with TBS, the sections were incubated with secondary antibody (biotinylated anti-goat IgG; Vector) at a dilution of 1:200 for 30 min at room temperature, followed by streptavidin (DAKO) at a dilution of 1:1000 for 15 min at room temperature. The sections were then rinsed twice in TBS, and then incubated in DAB solution for 5 min at room temperature.

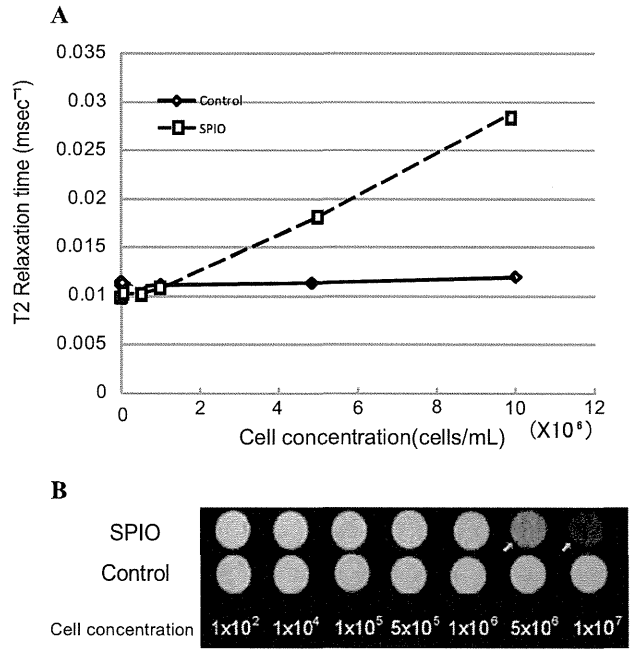

Fig. 2. Spectrometry of SPIO-labeled MSCs (SPIO) and unlabeled MSCs (control). (A) Graph showing the reciprocal of T2 relaxation time *versus* cell concentration. (B) T2 images of SPIO-labeled MSCs and control unlabeled MSCs *in vitro*. When cell concentration was greater than 5×10^6, the two indicated samples (arrows) differed according to low SI levels.

Please cite this article in press as: Watada, Y., et al., Magnetic resonance monitoring of superparamagnetic iron oxide (SPIO)-labeled stem cells transplanted into the inner ear. Neurosci. Res. (2015), http://dx.doi.org/10.1016/j.neures.2015.01.010